

**REPUBLIC OF IRAQ  
MINISTRY OF HIGHER EDUCATION  
AND SCIENTIFIC RESEARCH  
UNIVERSITY OF KARBALAA**



# **Fatigue Behavior of Polymeric Composite Materials Reinforced by Activated Carbon Particles.**

*A Thesis*

*Submitted to the Department of Mechanical Engineering*

*University of Karbala*

*In partial fulfillment of the requirements for the Degree of Master of  
Science in mechanical Engineering / applied mechanic*

*By*

***Qabas Razzaq Abdali***

*Supervised by*

***Asst. Prof. Dr.***

***Salah Noori Alnomani***

***Asst. Prof. Dr.***

***Mustafa Baqir Hunain***

بِسْمِ اللَّهِ الرَّحْمَنِ الرَّحِيمِ

اللَّهُ نُورُ السَّمَاوَاتِ وَالْأَرْضِ مِثْلُ نُورِهِ كَمِشْكَاةٍ فِيهَا مِصْبَاحٌ<sup>ط</sup>

الْمِصْبَاحُ فِي زُجَاجَةٍ

الزُّجَاجَةُ كَأَنَّهَا كَوْكَبٌ دُرِّيٌّ يُوقَدُ مِنْ شَجَرَةٍ مُبَارَكَةٍ زَيْتُونَةٍ لَا شَرْقِيَّةٍ

وَلَا

غَرْبِيَّةٍ يَكَادُ زَيْتُهَا يُضِيءُ وَلَوْ لَمْ تَمْسَسْهُ نَارٌ نُورٌ عَلَى نُورٍ

يَهْدِي اللَّهُ لِنُورِهِ مَنْ يَشَاءُ وَيَضْرِبُ اللَّهُ الْأَمْثَالَ لِلنَّاسِ

وَاللَّهُ بِكُلِّ شَيْءٍ عَلِيمٌ ﴿٣٥﴾

صدق الله العظيم

سورة النور

## Supervisors Certification

We certify that this dissertation entitled “Fatigue Behavior of Polymeric Composite Materials Reinforced by Activated Carbon Particles” was prepared by (Qabas Razzaq Abd-Ali) and had been carried out completely under my supervision at the University of Kerbala, Mechanical Engineering Department in partial fulfillment of the requirement for the degree of Master Science in Mechanical Engineering.



Signature

**Asst. Prof. Dr. Salah Noori  
Alnomani**

Mechanical Engineering  
Department University of  
Kerbala Data: 26/5/2021




Signature

**Asst. Prof. Dr. Mustafa  
Baqir Hunain**


Mechanical Engineering  
Department University of  
Babylon Data: / /2021

## Examining committee certificate

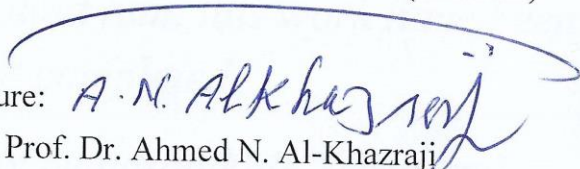
We certify that we have read this thesis entitled "Fatigue Behavior of Epoxy Composite Materials Reinforced by Activated Carbon Particles" and as an examining committee, examined the student, "Qabas Razzaq Abd-Ali", in its contents and that in our opinion it meets standard of a thesis for the degree of Master of Science in Mechanical Engineering.

Signature:   
Name: Asst. Prof. Dr. Essam Zuheir Fadhel  
Date: 10 / 5 / 2021

(Member)


Signature:   
Name: Lect. Dr. Ahmed Kasim Hassan  
Date: 10 / 5 / 2021

(Member)


Signature:   
Name: Prof. Dr. Ahmed N. Al-Khazraji

(Chairman)

Date: 11 / 5 / 2021


Signature:   
Name: Assit. Prof. Dr.  
Salah Noori Alnomani  
Date: 26 / 5 / 2021

(Supervisor)

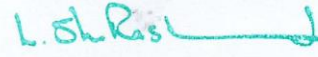
Signature:   
Name: Assit. Prof. Dr.  
Mustafa Baqir Hunain  
Date: / / 2021

(Supervisor)

Approval of the Department of Mechanical Engineering

Signature:   
Name: Dr. Hayder Noori Mohammed  
(Head of Mechanical Engineering Dept.)  
Date: / / 2021

Approval of Deanery of the College of Engineering University of Kerbala

Signature:   
Name: Assit. Prof. Dr. Laith Sh. Rasheed  
(Dean of College of Engineering)

## *Dedication*

*To ....*

*My mother, "Ibtisam Mohamed", the woman who raised me, the reason for all the beautiful things in my life.*

*The man who leaves us so early my father "Razzaq Abd-Ali".*

*The best partner, supporter, and best husband "Samir Mardan" without him, this work have been not completed*

*My happiness, my beautiful kids "Zoza and Hamoody."*

*My best friends, my sisters "Mayassa and Azal."*

*Qabas Razzaq*

# ***Acknowledgement***

*My gratitude is to Allah for everything ....*

*I pay my deep sense of gratitude to my supervisors: Asst. prof. Dr. Salah and Asst. prof. Dr. Mustafa. for their help, advice and support.*

*I express gratitude to my office, Babylon provincial council.*

*My gratitude goes to the Mechanical Engineering Department, University of Karbala and staff members of the Mechanical, Civil Engineering Department, College of Engineering, Babylon University, and materials engineering college.*

***Qabas Razzaq Abd-Ali***

***2021***

# ABSTRACT

Using natural reinforcement with polymer materials such as activated carbon (AC) as an alternative to synthetic reinforcement materials is an important topic nowadays. These plant-based reinforcements are degradable, eco-friendly, abundant and cheap, while synthetic reinforcement is expensive and negatively impacts the environments.

In this work, the effects of adding activated carbon (AC) powder with epoxy resin were investigated experimentally and numerically.

The particulate epoxy composites are manufactured using hand lay-up in vacuum technique with different weight fraction ratios of AC (0, 5, 10, 15, 20, 25, 30, 35 and 40) % wt. to find the best filling ratio which gives the highest mechanical and fatigue properties.

During this work, the particle size was measured by a laser particle size analyzer with an average size of about (14.74 $\mu$ m).

The interaction between epoxy material and AC powder was examined using Fourier Transform Infrared (FTIR) spectroscopy analysis. Moreover, the glass transition temperature ( $T_g$ ) of the pure epoxy and composite material were measured by Differential Scanning Calorimeter (DSC).

The tensile strength and fatigue of the composite's behavior were investigated experimentally and numerically; the fatigue behavior was described by S-N curves using the Basquin's Equation.

The ANSYS workbench software program carried the numerical work.

The composites' morphology and interaction between the matrix material and particles were investigated by conducting fracture surfaces of tensile and fatigue

specimens by (scanning electron microscope) (SEM) analysis to show the composites' fracture.

The FTIR test results reveal no new peak after reinforcing epoxy with AC powder, proving a strong interaction between the epoxy resin and AC powder. The Differential Scanning Calorimeter DSC results show that the increase in AC powder fraction led to an increase in glass transition temperature ( $T_g$ ) with percentage of increment 30.5% .

The FTIR analysis findings were supported by SEM analysis, which shows a good interaction and strong interfacial between matrix and powder.

The tensile strength values increased with increasing AC content up to 15 % wt. with a max value of 26.34 MPa increased by (18.87%), then it decreased to 18.15 MPa at 40 % wt. The ultimate fatigue strength was also increased with increased AC particles contents to reach the max value at 15% wt, increased by (18.18%).

3D finite element technique was used to model fatigue test numerically using ANSYS workbench program 16 to compare the S-N curves have the same behavior and the maximum percentage difference as does not exceed (4.43 %). Also, this program was used to find available fatigue life, safety factor, and Von Mises stresses in specimens

Finally, the (SEM) was used for morphological inspection to investigate the tensile and fatigue failed specimens' microstructure to show the fracture's nature.



# LIST OF CONTENTS

<b>Subject</b>	<b>Page No.</b>
Abstract	I-II
List of Contents	III-VI
List of Figures	VII-X
List of tables	XI
Nomenclature	XII
Abbreviations	XIV
<b>Chapter One: introduction</b>	
1.1 General	1
1.2 Particulate polymer composites	2
1.2.1 Why epoxy reinforced with activated carbon particles	2
1.3 Fatigue failure	3
1.4 Research objectives	4
1.5 Work limitation	4
1.6 Thesis layout	4
<b>Chapter Two: Literature Review</b>	

2.1 Introduction	6
2.2 The effect of weight fraction and one type of microparticles on mechanical properties	7
2.3 The effect of different types of particles on the same polymer on mechanical properties	9
2.4 The effect of particles on fatigue behavior of the particulate composite	12
2.5 Concluding Remarks	13
<b>Chapter Three: Theoretical Consideration and Numerical Investigation</b>	
3.1 Particulate composites	15
3.2 The law of mixtures	15
3.3 Fatigue failure	16
3.4 Basquins equation	17
3.5 Numerical Model	18
3.6 Stress life Method	18
3.7 Ansys workbench	18
3.7.1 Analysis steps	19
3.7.1.1 Building the Model	20
3.7.1.2 Element type	20
3.7.1.2 Defining the Material Properties	21
3.7.1.3 Meshing	21
3.7.1.4 Define the Analysis Type and boundary conditions	22
3.7.1.5 Solution and results	23

<b>Chapter Four: Experimental Work</b>	
4.1 introduction	24
4.2 Material	25
4.3 Composite fabrication	28
4.4 Experimental setup	32
4. 4. 1 Particle size analyzer	32
4.4.2 Fourier transform infrared spectroscopy (FTIR)	33
4.4.3 Differential scanning calorimetry (DSC)	34
4.4.4 Tensile test	35
4.4.5 Fatigue test	36
4.4.6 Scanning electron microscope (SEM)	40
<b>Chapter Five: Results and Discussion</b>	
5.1 Introduction	41
5.2 Particles measurement	41
5.3 Fourier-transform infrared spectroscopy (FTIR) results	42
5.4 Results of Differential scanning calorimetry (DSC)	44

0

2

3

4

5

6

7

8

5.5 Tensile test result	45
5.6 Results of the Scanning electron microscope (SEM) of fractured surfaces of tensile specimens	48
5.7 Results of Fatigue Tests	51
5.7.1 Experimental results	51
5.7.2 Numerical results	53
5.7.3 Comparison between experimental and numerical results	54
5.7.4 Contour plot by ANSYS workbench	56
5.7.5 SEM results for fracture surface of fatigue specimens	63
<b>Chapter Six: Conclusion and Recommendation</b>	
6.1 Introduction	66
6.2 Conclusions	66
6.3 Recommendation for Future Work	67
<b>References</b>	68
<b>Appendix</b>	A-1

## LIST OF FIGURES

Figure Number	Subject	Page
3.1	Fatigue fracture surface	16
3.2	fatigue loading	17
3.3	S-N curve	18
3.4	Flow chart of Ansys workbench	19
3.5	Model Geometry	20
3.6	SOLID186 Homogenous Structural Solid Geometry	20
3.6	Properties of material	21
3.7	Meshing	22
3.8	The model and boundary condition	22
4.1	Flow chart of the experimental work procedure	24-25
4.2	Activated carbon particles	26
4.3	Vibrating sieve	28
4.4	Vacuum device	29
4.5	Tensile mold	29
4.6	Fatigue mold.	30
4.7	Samples in the oven.	30

<b>4.8</b>	Tensile specimens	31
<b>4.9</b>	Fatigue specimens.	31
<b>4.10</b>	Particle size analyzer	32
<b>4.11</b>	Fourier-transform infrared spectroscopy (FTIR)	34
<b>4.12</b>	Differential scanning calorimetry (DSC)	35
<b>4.13</b>	Universal tensile testing machines.	36
<b>4.14</b>	tensile specimen according to the specification of ASTM 638	36
<b>4.15</b>	Fatigue test specimens according to ASTM WP-140 specifications	37
<b>4.16</b>	The load on a clamped specimen	37
<b>4.17</b>	Fatigue machine	39
<b>4.18</b>	Scanning electron microscope (SEM).	40
<b>5.1</b>	The size distribution of AC particles	42
<b>5.2</b>	FTIR spectra of all specimens, where the x-axis represent wavelength in (1/cm) and the y-axis represent the absorbance (Abs)	43
<b>5.3</b>	Stress-strain diagram for pure epoxy and its composites	46
<b>5.4 (a) and (b)</b>	The relation between ultimate tensile strength, modulus of elasticity with AC % content	47

<b>5.5</b>	Micrographs by Scanning electron microscope (SEM) images of fracture surfaces of tensile specimens for (a) 10 % wt. of activated carbon (b) 15 % wt. of activated carbon (c) 20 % wt. of activated carbon.	50
<b>5.6</b>	Experimental S-N curves of epoxy composite reinforced with activated carbon particles with weight ratio (0,10,15,20%)	52
<b>5.7</b>	Numerical S-N curves of epoxy composite reinforced with activated carbon particles with weight ratio (0,10,15,20%)	53
<b>5.8</b>	Comparison between experimental and numerical S-N curve for 0% wt. fraction.	54
<b>5.9</b>	comparison between experimental and numerical S-N curve for 10% wt. fraction.	55
<b>5.10</b>	Comparison between experimental and numerical S-N curve for 15% wt. fraction	55
<b>5.11</b>	Comparison between experimental and numerical S-N curve for 15% wt. fraction.	56
<b>5.12</b>	Contour plot of equivalent Von-Mises stress at R=-1	59

<b>5.13</b>	Contour plot of the safety factor, where the maximum safety factor displayed is 15 at stress ratio $R=-1$ .	61
<b>5.14</b>	Contour plot of the life obtained for the analysis of fatigue at stress ratio $R=-1$ .	63
<b>5.15</b>	Micrographs by Scanning electron microscope (SEM) images of fracture surfaces of fatigue specimens for (a) 0 % wt. of activated carbon (b) 10 % wt. of activated carbon (c) 15 % wt. of activated carbon (d) 20 % wt. of activated Carbon	64
<b>5.16</b>	Micrographs by Scanning electron microscope (SEM) images of fracture surfaces of fatigue specimens for (a) 10 % wt. of activated carbon (b) 15 % wt. of activated carbon (c) 20 % wt. of activated carbon.	65



## LIST OF TABLES

Tables	Subjects	Page
4.1.	Standard properties of epoxy	26
4.2.	Standard properties of activated carbon particles	27
5.1	Glass transition temperature for neat epoxy and epoxy composite	45
5.2	The effect of activated carbon % wt. on tensile tests	48
5.4	Experimental S-N curves equations (Basquin's equation) and correlation coefficient for (0,10,15,20%) wt. of activated carbon particles.	52
5.5	Numerical S-N curves equations (Basquin's equation) and correlation coefficient for (0,10,15,20%) wt. of activated carbon particles.	54

## NOMENCLATURE

Symbols	Description	Unite
$A$	The fatigue strength coefficient	--
$A$	Bending arm	Mm
$B$	The fatigue strength exponent	--
$D$	The diameter of the specimen	Mm
$E$	Modulus of elasticity	GPa
$F$	Applied load	N
$M$	Bending moment	N.mm
$N_f$	The number of cycles to failure	--
$R$	Stress ratio	MPa
$S$	Fatigue strength	MPa
$T_g$	Glass transition temperature	°C
$W$	Section modulus of the specimen	$m^3$
$\Sigma$	Maximum alternating stress	MPa

## GREEK SYMBOLS

Symbols	Description	Unite
$\rho_c$	Composite density	Kg/m <sup>3</sup>
$\rho_m$	matrix density	Kg/m <sup>3</sup>
$\rho_p$	particles density	Kg/m <sup>3</sup>
$\sigma_a$	Stress amplitude	MPa
$\sigma_m$	Mean stress	MPa
$\sigma_{ult}$	Ultimate tensile strength	MPa
$\sigma_{ult}$	Ultimate tensile strength	MPa

## ABBREVIATIONS

Abbrev.	Description
AC	Activated Carbon
ATH	alumina trihydrate
CH <sub>2</sub>	Methylene.
CH <sub>3</sub>	Methyl group
Cumulative.	Cumulation
Diffra.	Diffraction.
DSC	Differential Scanning Calorimeter
FTIR	Fourier Transform Infrared
ILSS	Interlaminar Shear Strength
MAPO	maleic anhydride and peroxide
$m_c$	Mass of composite
$m_m$	Mass of matrix
$m_p$	Mass of particles
OH	Hydroxide
PMMA	Poly Methyl Methacrylate
$T_g$	Glass transition temperature
SEM	Scanning Electron Microscopy
$V_c$	The volume fraction of the composite
$V_m$	The volume fraction of the matrix
$V_p$	The volume fraction of particles
$v_c$	Composite volume
$v_m$	Matrix volume
$v_p$	Particles volume

---

# CHAPTER ONE

## Introduction

### 1.1 General

Classic material like metals and metal alloy becomes insufficient in modern industries requirements; thus, creating material with specific characteristics is necessary.

Composite material provides low density, high fatigue strength, toughness, high resistance to friction and wear, good mechanical and thermal properties. Lightweight other important property enables the composite to use it in lightweight applications such as aircraft, aerospace, automobile structures, biomedical, civil, space, underwater vehicles, marine, pressure vessel, medical device, sports, and other mechanical engineering components.

Composite material defines as a material consisting of two or more physically or chemically distinct phases and having different interphase separating them. One of these phases, called reinforcement, plays a significant role in carrying the load, applying composite material, and improving its properties. The other called matrix, where the reinforced imbedded in it. The matrix insulates the fibers from one another to avoid abrasion and prevent new surface defects from forming. The matrix acts as a bridge to keep the fibers in their places. A useful matrix should deform easily under applied load, transfer the load onto the fibers, and evenly distribute stress concentration [1].

Composite classify with respect its contents: matrix and reinforcement, composite types depending on the matrix:

- 1- Metal matrix composites.
- 2- Ceramic matrix composite

3- Polymer matrix composite.

Composite which classify concerning reinforcement:

- 1- Structure composite which divided to sandwich laminate.
- 2- Fibrous composite.
- 3- Particulate composite [2].

## **1.2 Particulate polymer composites**

The reinforcement in the particulate composite is particles embedded in the matrix. The most popular matrix is polymer because of its low density, the fabrication process is easy and low cost compared with metal and Ceramic matrix, also the polymer matrix have a good thermal and chemical resistance, good strength, and stiffness properties [3] polymer composites application is so spacious and incredibly lightweight.

Particles used to improve polymer properties reduce the cost and simplify composite manufacturing [4]. According to the particle's properties, its effect will be on the composite's properties: mechanical properties (tensile strength, hardness, fatigue strength), physical properties, and thermal properties, also particles simplify composite fabrication and reduces costs of fabrication and composite compared with other reinforcement (fiber and laminate) [5].

For these particulate composite specifications, the epoxy used as polymer matrix and activated carbon particles as particulate reinforcement in this study.

### **1.2.1 Why epoxy reinforced with activated carbon particles**

Epoxy is one of the most important thermoset polymer matrices in the fabrication of advanced materials. Epoxy properties make it so important, like

---

high strength, low creep, good adhesion after curing, low viscosity, low shrinkage, low cost. It has good thermal, mechanical, and electrical properties, easy to fabricate in any shape, making it meet design requirements [6].

Activated carbon particles it is rich in carbon, as (87% to 97%) of it is carbon with a high surface area larger than 1000 m<sup>2</sup>/ gm due to its porous structure [7] and pore diameter is less than 0.6 cc, making it excellent absorbent. This porosity enables the polymer matrix material to penetrate inside, making high bonding. Besides that, the low cost, low density, low energy consumption, high mechanical strength, and easily repeated generation comparing with fiber and laminate are significant factors to use as polymer fillers in developing mechanical properties of polymers. The use of activated carbon helps in profiting from agricultural residues such as coconut shells, nutshell, coal, peat and wood olive stones and walnut shell, cherry stones, rice bran, jackfruit shell waste and oil palm shell which solve the waste disposal [8].

These composite applications can be used widely in different fields to replace heavy materials in engineering structures, especially in automobile and aerospace industries, ships, boats, electrical isolation, marine application, sports parts, and construction [8].

### **1.3 Fatigue failure**

Fatigue is the most important failure that occurs in materials, including composites. This failure happens due to repeating load cyclically and occurs suddenly without warning [9]. The source of 80% of failure cases is fatigue failure, because of that fatigue strength is considered a material property, for this reason, the study of fatigue failure studying is significant to[10]:

1. Predict the material's behavior in the future and its age to reduce this failure's risks.

2. Obtaining the endurance limit and safety factor for pure epoxy and epoxy –AC composites .

### **1.4 Research objectives**

1. Examine the effect of weight fraction of micro activated carbon to the epoxy matrix on the strength and fatigue strength composite of composite material experimentally and numerically.
2. Finding the best value in tensile and fatigue tests .
3. Determine the interaction between AC particle and epoxy material using the Fourier Transform Infrared (FTIR) spectroscopy analysis.
4. Find the glass transition temperature (T<sub>g</sub>) of the pure epoxy and composites by using Differential Scanning Calorimeter (DSC)
5. Scanning Electron Microscopy (SEM) analysis was also performed to take some information about tensile strength, fatigue fracture surface and strength of the interaction between AC and matrix material.

### **1.5 Work limitation**

1. Experimental tests in this thesis and numerical work were done in this thesis.
2. Using one type of reinforcement activated carbon particles with an average size of about 14.74  $\mu\text{m}$ .
3. Using one type of polymer matrix material (epoxy).
4. The weight fractions of AC particles to epoxy resin (0,5,10,15,20,25,30,35,40%) wt. for tensile, FTIR tests, and DSC tests;(0,10,15,20%) wt. for fatigue tests.

### **1.6 Thesis layout**

In chapter one, an introduction to the subjects of the thesis.

In chapter two, the literature review.



In chapter three, theoretical consideration and numerical investigation.

In chapter four, experimental work.

In chapter five, the results and discussions of numerical results and experimental results.

In chapter six, the conclusion and recommendation.

In appendix A-1, Differential Scanning Calorimetry DSC Results.

# CHAPTER TWO

## literature Review

### 2.1 Introduction

The composite material has high specifications and provides many industrial requirements. Therefore, many researchers studied the properties of the composite.

Particulate composite reinforced with natural particles has significant interest from researchers due to low cost and easy fabrication compared to other reinforcements. These reinforcements are degradable, eco-friendly, abundant and cheap, while synthetic reinforcement is expensive and negatively impacts the environments [10].

In the literature review of this work, an overview is given of the natural particles' materials used as reinforcement and effectiveness in enhancing the polymer's mechanical properties (mechanical properties, fatigue strength).

In this review, three parts are covered; the first part includes the effect weight fraction of one particle type on mechanical properties. The second part consists of different kinds of particles on the same polymer with mechanical properties. And the third the effect of particles on the fatigue behavior of the particulate composite .

---

---

## 2.2 The effect of weight fraction and one type of micro particles on mechanical properties

**J. Olumuyiwa Agunsoye et al. [11], 2012**, studied mechanical properties of polyethylene reinforced with coconut shell particles with volume fraction (5%-25%) wt. and particle size 100  $\mu\text{m}$ ., the results reveal that the hardness is increasing with the increasing of coconut shell particles. The tensile strength modulus of elasticity decreased, and the composite with the highest volume fraction of filler (25%) wt. The lowest strength (6.59 MPa) due to Scanning Electron Microscopy (SEM) results revealed the composites' surfaces had poor interfacial interaction between the coconut shell particle and the matrix.

**Salleh Z. et al. [12], 2013**, Studied the effect of Activated Carbon (AC) composites prepared from carbon coconut shell reinforced with polypropylene (PP) on tensile properties. The carbon coconut shell was selected from coconut shell specifically namely as carbon Komeng coconut shell (CKCS with weight fraction (6%,4%,2%) and polypropylene with weight fraction (4%,6%,8%) encapsulated with epoxy resin, the results reveals that the tensile stress developed when activated carbon increased. Maximum tensile stresses were in (PP 4wt% + AC 6wt%) composite. SEM Microphotographs of the selected samples for AC + PP composite Showed agglomeration with AC granules. The impact strength increased when polypropylene increased, and the maximum increment was PP-6wt%+AC4wt%.

**C.U. Atuanya et al. [13], 2014**, studied the effect of breadfruit hull ash as reinforcement with a weight ratio from 5 to 25% with size 2  $\mu\text{m}$  on microstructure and mechanical properties of recycled low-density polyethylene. The results reveal that the properties increase with increasing filler weight ratio where the tensile strength increased from 6.5 MPA at (0 wt%) to a maximum of

---

12.40 MPA at (20 wt.%) was the best improvement. Successful fabrication, uniform distribution, good interfacial bonding between the polymer and the breadfruit seed hull ash fillers proven by SEM Microphotographs contributed to an increment in tensile properties.

**Md. Mahfujul Islam et al. [14], 2015**, Investigated rice husk ash's effectiveness as reinforcement of polyester composite material's mechanical properties with weight fraction (0,5,10,15, 20%). The results show that flexural strength declined when the filler weight ratio increased, the elastic modulus of flexural strength increased until 5% wt. fraction then decreased, compressive strength composite decreases with the increase of rice husk ash. Cavities formed in the composite was the reason for reducing mechanical properties.

**Jassim Mohammed Salman [15], 2015**, studied the effect of carbon black (CB) particles with size (14  $\mu\text{m}$ ) and weight fraction (5,7.5,10%) imbedded in the polyester matrix on mechanical properties. The results reveal that the maximum tensile strength, which was in 10% Carbon Black, the best value of hardness was at 10%wt (CB), impact strength was improved at 7.5%wt, flexural strength was improved at the same percentage of tensile strength. This development attributed to better dispersion of carbon black in the polyester matrix, better wettability and interfacial bond.

**Iftekharul Islam et al [16], 2017**, Studied the effect of carbon black (CB) particles with weight fraction (0,5,10,15,20,25,30%), particles size ranging from 125 to 177  $\mu\text{m}$ . imbedded in polyvinyl chloride (PVC) on tensile properties, the results reveal that tensile properties increased when particles fraction increased the tensile properties of CB-PVC composites showed that the tensile strength of the composites increased with an increase in CB loading up to 15% wt., and then decreased. Still, elongation at break decreased with increasing CB, after 15%wt. fraction the properties decreasing. Particles tend to

agglomerate at high filler contents of more than 15 wt. %, resulting in improper bonding between the CB and the PVC

**Thaís da Costa Dias et al. [17], 2018**, Investigated the effect of carbon wastes powder to reinforce the epoxy matrix in different weight fraction (0, 2.5, 5, 7.5, 10%) on mechanical properties with particle size at the range of (149-74 $\mu$ m), the results reveal that the addition of carbon powder makes development in tensile strength up to 30.% for 5% wt. composite, tensile modulus up to 36.6 for 7.5% wt. composite; the compressive strength increased up to 19% for 5% wt. composite, the flexural strength increased up to 22% for 7.5% wt. composite. Therefore, the material becomes more brittle and dramatically reduces the impact strength by 55% for all waste mass fraction levels considered tensile strength.

**Samuel Audu Seth et al. [18], 2019**, studied the effect of Doum palm shell particles as reinforcement on physical and mechanical properties of polypropylene with weight ratio from 0% to 40% and particles sieved at 150 and 300  $\mu$ m, the results reveal that the highest value of impact strength for 150  $\mu$ m was at 35% wt. fraction, for 300  $\mu$ m, the highest value of impact strength was at 30 % wt. fraction and the impact strength of 150 $\mu$ m were higher than 300 $\mu$ m particle size (4.1 kJ/m<sup>2</sup> ), resulting in hardness.

### **2.3 The effect of different types of particles reinforced polymer materials on mechanical properties**

**H.P.S. Abdul Khalil et al. [19], 2007**, studied the effect of adding carbon black and activated carbon were produced from bamboo with weight ratio (10,20, 30, 40%) wt. fraction with particle size (100, 300, and 425  $\mu$ m) reinforced polyester matrix on physical and mechanical properties. The results reveal that the water absorption slightly increased as filler loading increased,

---

tensile and flexural strength, elongation at break, toughness and impact properties decreased as filler loading increased.

**Dalila Laouchedi et al. [20],2017**, Studied the effect of two types of clay powder: kaolin and metakaolin (treated) in the epoxy matrix with volume fraction (2%-20%) on mechanical properties. The results reveal that increasing the tensile strength and Young's modulus with a decrease in deformation. Young's stress modulus's best outcome is obtained at 18% filler rates, with a minimum elongation value at the break when both types of clay are added. Still, the treated one (metakaolin) showed better properties than kaolin because it offered better interaction.

**Orhan S. Abdullah[21], 2017**, investigated the effect of natural particles (sunflower husk and pomegranate husk particles) on tensile properties of the polyester composite, with weight fraction (3,7,10%) and particles size (50 $\mu$ m, 100  $\mu$ m and 150  $\mu$ m), the results reveal that the tensile strength increasing with the increase of weight fraction of particles, the best value was for pomegranate husk particles-polyester composite at 7% wt. fraction, and best value for sun flower-polyester composite at 10% wt. fraction, which is better than pomegranate composite. The decrease in reinforcement material particle size led to an increase in the tensile strength, Young's modulus and water absorption in the two types of particles.

**K. Harrimaniid and I. SitiRabiatull Aisha [22], 2012**, studied the effect of adding rice husk as filler on tensile properties of polyester composite with weight ratio (10, 15, 20 and 25%); the results reveal that tensile properties decreased when the filler loading was increased until 25% wt. fraction the tensile strength increased, the Young modulus increased until 15% wt. fraction then deceased, this disparity in results is caused by weak bonding between the natural particles and the polymer, causes a decrease in the tensile strength when

---

the filler loading increases. Also, low dispersion causes agglomeration of the fillers as well as decreasing the tensile properties.

**Shakuntyala Ojha et al [23], 2012**, studied the effect of orange peel particles as filler on epoxy composites' mechanical properties with particle size 212  $\mu\text{m}$  and weight fraction (0,5,10,20,30%). The results reveal that the tensile strength increased by 20% wt. fraction, which was (25.85 MPa) then slightly decreased, similar in the flexural strength, which had the best value in 20% wt. fraction which is (62.35 MPa), best hardness was in 20% wt. fraction too, which is (20.72), these results confirmed by SEM Micrographs reveal that no debonding, no particle is chipping out, and no crack formation shows that the bonding is strong between the matrix and reinforcement.

**Ojha Shakuntala et al [24], 2014**, studied the effect of (5, 10, 15, 20%) wt. fraction of wood apple shell particles with particle size 212  $\mu\text{m}$  on the epoxy composite's mechanical and tribological properties reveals that the tensile strength increased until 15% wt. fraction then decreased, flexural strength also increasing until 15% then decreased. Interlaminar Shear Strength (ILSS) also had the best value at 15% wt. that indicated better interfacial interaction and effective load transfer between filler and epoxy resin due to better dispersion. Fraction and erosive wear resistance strength increased with the increasing the particles. The loading of 15% was the best.

**Raghad Usama. Abass [25], 2015**, studied the effect of orange peels particles on polyester composites' mechanical properties with weight fraction (2, 4, 6, 8 and 10%). The results reveal that the impact strength had a maximum of 10% wt. fraction of orange powder, the hardness value of the composite increases with increasing filler content. The tensile strength of the composite is found to be maximum for the 10 % wt. fraction, the compression test of the composite is found to be maximum at 10%wt. fraction.

---

**Kamila Salasinska et al. [26], 2018**, studied the effect of walnut shell (WS) particles with weight ratio (20, 30, 40, and 50 %) with particle size (32–125  $\mu\text{m}$ ). On mechanical and thermal properties, the results reveal that the tensile strength and impact resistance decreased when fillers loading increased; FTIR spectra showed the sample containing 50 wt.% of WS showed a substantial decrease in absorbance at this intensity. Therefore, it can be stated that the presence of the organic filler modified the curing process.

**Reem Alaa Mohammed and Ahamed Al-Ghabban [27], 2019**, studied the effects of orange peels particles on Poly Methyl Methacrylate composites' mechanical properties with weight fraction (2%, 4%, 6%, and 8%). The results reveal that the 8% wt. of orange peels powder causes increasing in modulus of elasticity, flexural strength and flexural modulus, the 4%wt. of orange peels powder had a maximum of tensile strength, elongation percentage 8% wt. of orange peels powder compared to others, the impact strength values increased by 6% wt. of orange peels powder. In contrast, the impact strength decreased in 8%wt of orange peels powder.

## **2.4 The effect of particles on fatigue behavior of the particulate composite**

**Md Minhaz [28], 2019**, studied fatigue analysis of polypropylene (PP) reinforced with wood flour with a weight fraction of 10% wt., the fatigue test of the composites was also conducted at conditions of 25 °C and 40% RH, fatigue load was tension-tension, and stress ratio (0.1). The results revealed that the neat polypropylene (PP) had fatigue strength lower than composites contain wood flour particles.



---

**Mohammed Hussein B. Hassan and Ekram. A.AL-Ajaj [29],2016**, studied the effect of chopped carbon fiber (length 8 mm and diameter 4.2  $\mu\text{m}$ ) on fatigue behavior of epoxy composite with weight fraction (2.5%,5%,7.5%,10%,12.5%) wt., fatigue test had been established at stress ratio  $R=-1$  (reversed load), the results reveal that the fatigue strength, fatigue limit and fatigue life increases with the increase in a weight ratio of filler, for all composite until 12.5% wt. which fractured rapidly due to the debonding of the chopped carbon fibers from the matrix epoxy.

**M.M. Shokrieh et al. [30], 2014**, studied the effect of various weight fractions of graphene nanoplatelet (GPL) (0.1, 0.25, 0.5 wt. %) on flexural fatigue behavior of epoxy polymer has been investigated at room temperature. The results reveal that the increase of graphene nanoplatelets led to the rise in epoxy fatigue and 0.25 wt. % of graphene nanoplatelet on fatigue life was the best 27.4 times improvement in flexural bending fatigue life of the neat epoxy because of a uniformed dispersion of graphene nanoplatelets was observed by Scanning Electron micro Scopey (SEM) image of the fracture surface of the specimen of 0.5 wt. % GPL/epoxy nanocomposites

## 2.5 Concluding Remarks

From the review studies, the following was concluded:

1. The matrix-type, particles type, size, dispersion, and weight fraction affect the particulate composite materials' mechanical properties and fatigue strength.
2. Natural particles can be a good reinforcement with polymers if appropriately used.
3. At a high weight ratio, the mechanical properties decreased.

The present study is different from the published work by using The Fourier Transform Infrared (FTIR) spectroscopy analysis to check out the interaction between reinforcement and polymer matrix, Differential Scanning Calorimeter (DSC) has been carried out to find the glass transition temperature  $T_g$  of the pure epoxy and composites, and investigated particles effect on fatigue properties and verification it by using finite element methods .

## CHAPTER THREE

### Theoretical and Numerical Consideration

#### 3.1 Particulate composites

It's an important example of modern composite, which depends on matrix specifications and reinforcement (particles) specifications such as the dimension of the particles, the interparticle spacing, the weight fraction of the particles, the direction of particle distribution, the bonding between the particles and the matrix, mechanical properties of particles.

In this work, the particles dispersed in the matrix randomly; the particles are different in size and shape; the bonding between matrix and particles is strong; the composite .

#### 3.2 The law of mixtures

The sum of matrix mass and filler mass which is in this research particles equal to composite mass.[31]

$$m_c = m_m + m_p \quad (3.1)$$

$$v_c \rho_c = v_m \rho_m + v_p \rho_p \quad (3.2)$$

$$\rho_c = \frac{v_m}{v_c} \rho_m + \frac{v_p}{v_c} \rho_p \quad (3.3)$$

$$V_m = \frac{v_m}{v_c}, V_p = \frac{v_p}{v_c} \quad (3.4),(3.5)$$

$$\rho_c = V_m \rho_m + V_p \rho_p \quad (3.6)$$

$$v_c = v_m + v_p \quad \text{divided by } v_c \quad (3.7)$$

$$1 = \frac{v_m}{v_c} + \frac{v_p}{v_c} \quad (3.8)$$

$$1 = V_m + V_p \quad (3.9)$$

$$V_m = 1 - V_p \quad (3.10)$$

$$V_p = \frac{m_p}{\rho_p v_c} \quad (3.11)$$

So, the density equation concerning volume fraction of filler and density of matrix and particles:

$$\rho_c = \rho_m(1 - V_p) + \rho_p V_p \quad (3.12)$$

### 3.3 Fatigue failure

It is a kind of failure that occurs in materials, and it happens as a result of repeating load cyclically [32]. Fatigue is the most critical failure in materials, including composites, where fatigue is the source of 80% of failure cases and happened without warning [33]. The starting of fatigue is from points in which stress concentration, such as sharp edges, small crack on the surface, defect and flaws within the materials. As a result of cyclic load, discourtesies occur in molecular structure. Plastic deformation, then a small crack formed, is the first stage of fatigue. In the second stage, the crack developed. The final stage is the fracture of material, which can be brittle or ductile [33]. The fracture surface consists of a smooth part contains a beach mark, each period of the crack's progress is represented by a ring whose center is the beginning of the crack, and the rough part represents the fracture area [34].

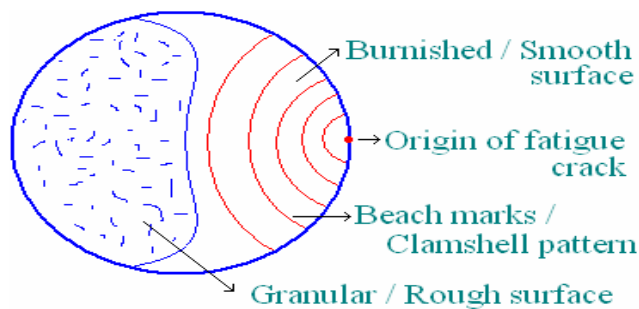


**Figure 3.1** Fatigue fracture surface [34]

Fatigue loading types depend on minimum stress to maximum stress, which called stress ratio (R), in this work stress ratio is (R = -1) when the compressive stress amplitude equal tensile stress amplitude. This called reversed loading; a rotating shaft is an example of this type.

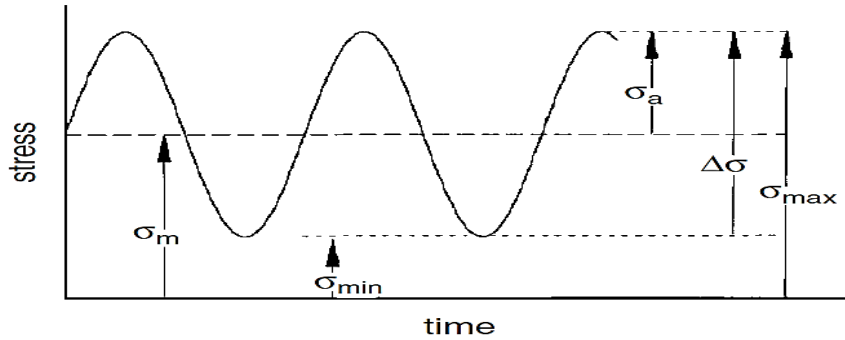


**Figure 3.2** fatigue loading [35]

$$\text{Constant stress range: } \Delta\sigma = \sigma_{max} - \sigma_{min} \quad (3.13)$$

$$\text{Mean stress: } \sigma_m = (\sigma_{max} + \sigma_{min}) / 2 \quad (3.14)$$

$$\text{Stress amplitude: } \sigma_a = (\sigma_{max} - \sigma_{min}) / 2 \quad (3.15)$$

$$\text{Stress ratio: } R = \sigma_{min} / \sigma_{max} \text{ in our case, } R = -1 \quad (3.16)$$

$$\text{Amplitude ratio: } A = \sigma_a / \sigma_m \quad (3.17)$$

Fatigue life prediction is usually made using the S-N curve. The y axis represents the cyclic stress amplitude; the x-axis represents the number of cycles until the material fails. when the material is ferrous, the curve decreasing until it reaches a specific limit called endurance limit, the non-ferrous material has no endurance limit [35]

### 3.4 Basquin's Equation

S-N curve is the relationship between the y axis represents the cyclic stress amplitude. The x-axis represents the number of cycles until the material fails on a logarithmic scale.

Basquins equation is a power law, show the relationship between fatigue strength and the number of cycles to failure.

$$\sigma_a = A(N_f)^B \quad (3.18)$$

$\sigma_a$  = stress amplitude

A=constant = The fatigue strength coefficient.

$N_f$  = The number of cycles to failure

$B = \text{constant} =$  The fatigue strength exponent.

The coefficients can be obtained using the least square method (linearizing the power law in a logarithmic form).

### 3.5 Numerical Model

The method that used in this work is the stress life method .

#### 3.5.1 Stress life Method

this method is widely used in high cycle fatigue application. In such an application, the stress in the elastic range of material gives higher fatigue life. It's done using the S-N curve, which shows the relationship between cyclic stress amplitude and the number of cycles until the material fails. When a material is ferrous, the curve decreasing until it reaches a specific limit called fatigue limit, the non-ferrous material has no fatigue limit [36].

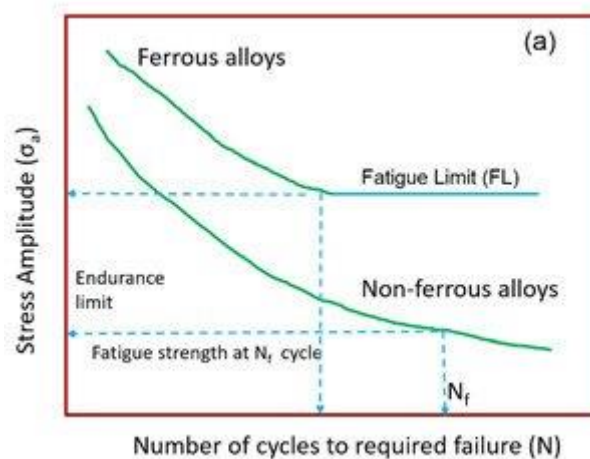


**Figure 3.3** S-N curve [36]

### 3.6 Ansys workbench

In the present work, ANSYS Workbench software (version 16) was used in modelling fatigue test to simulate and estimate the fatigue life for epoxy

composite reinforced with activated carbon particle with weight ratio (0,10,15,20%) with stress ratio ( $R=-1$ ) based on stress Life.

### 3.6.1 Analysis steps

ANSYS workbench used to make the simulation of the required model. It has three clear steps: building the geometry as a model, applying the boundary conditions (loading, supports..... etc.), obtain the solution and give the results.

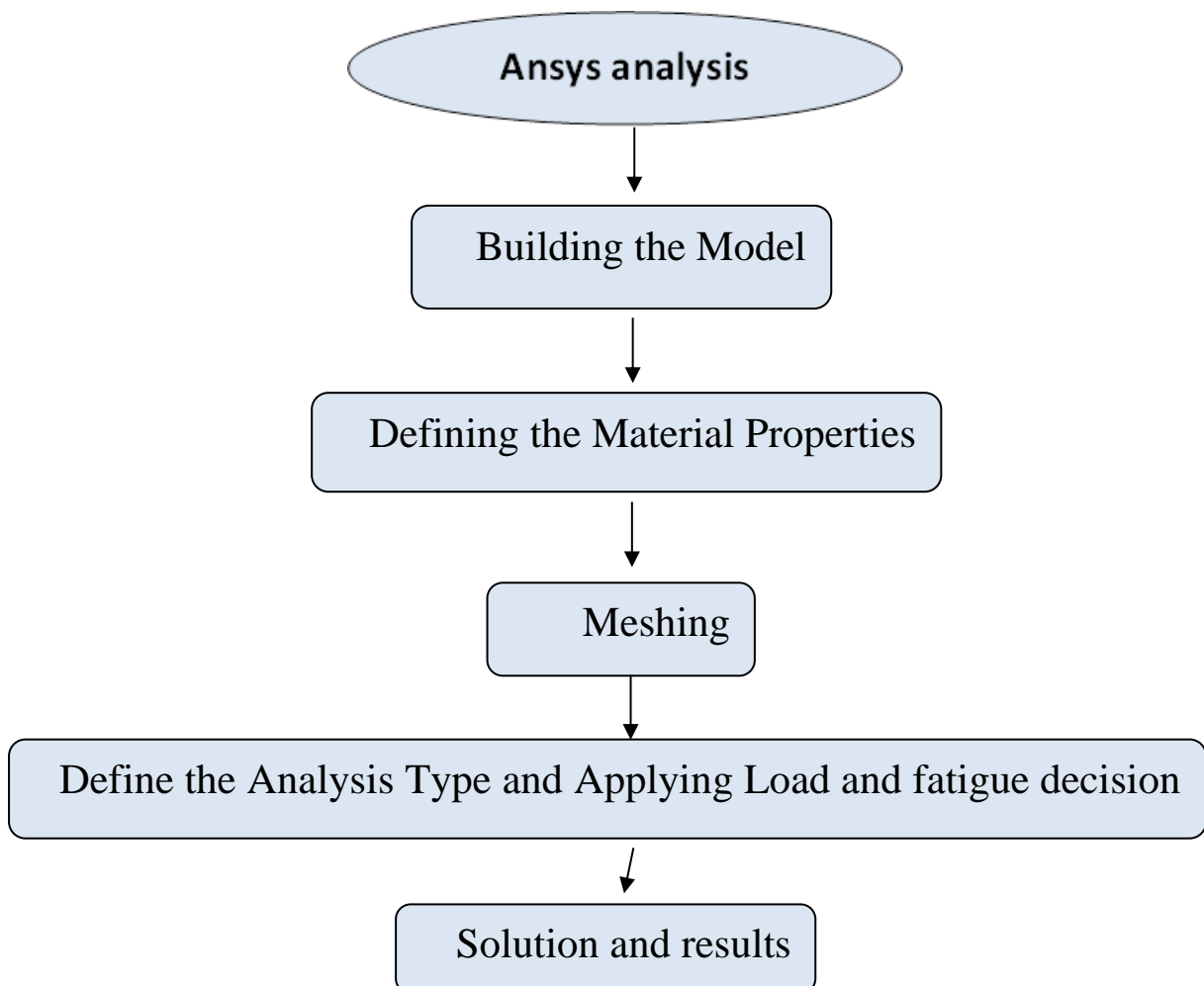


**Figure 3.4** Flow chart of Ansys workbench.

#### 3.6.1.1 Building the Model

In the present work, the model export from Auto Cad for simplicity.

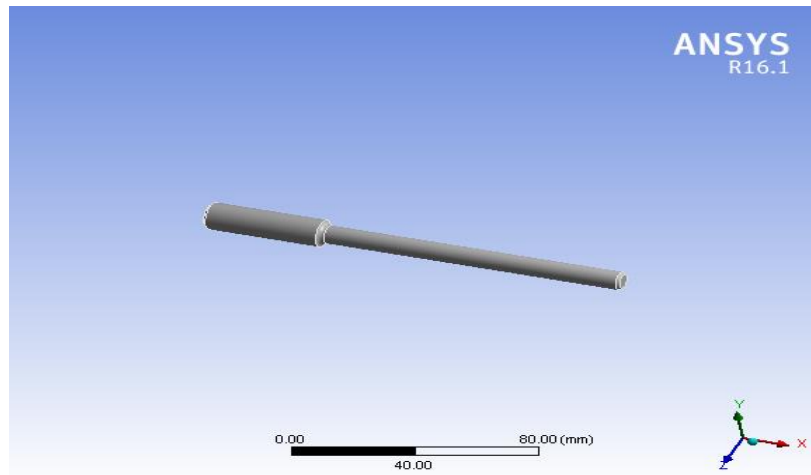


**Figure 3.5** Model Geometry

### 3.6.1.2 Element type

SOLID186 is a higher-order 3-D 20-node solid element that exhibits quadratic displacement behavior. The element is defined by 20 nodes having three degrees of freedom per node: translations in the nodal x, y, and z directions. The element supports plasticity, hyper elasticity, creep, stress stiffening, large deflection, and extensive strain capabilities [37].

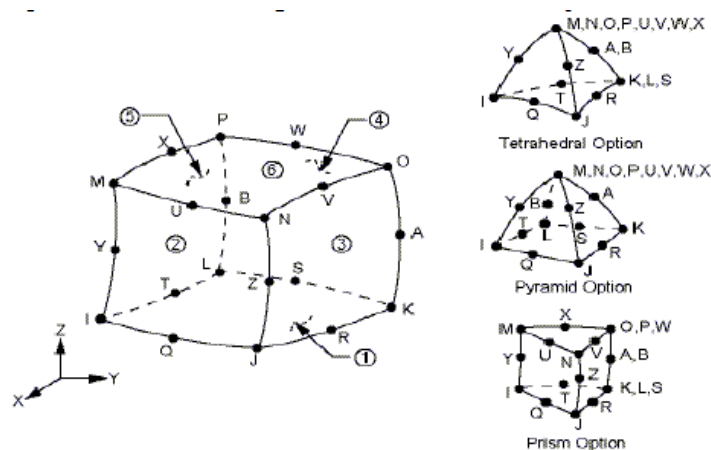


**Figure 3.6** SOLID186 Homogenous Structural Solid Geometry [37].

### 3.6.1.3 Defining the Material Properties



The linear isotropic information and mechanical properties of the model obtained from the experiments should be recorded to simulate the model. To make fatigue simulation, the required data shown in figure 3.6 was taken from experiments.

Properties of Outline Row 4: 0%				
	A	B	C	D E
1	Property	Value	Unit	
2	Density	1100	kg m <sup>-3</sup>	
3	Isotropic Elasticity			
4	Derive from	Young's Modu...		
5	Young's Modulus	1010	MPa	
6	Poisson's Ratio	0.34		
7	Bulk Modulus	1.0521E+09	Pa	
8	Shear Modulus	3.7687E+08	Pa	
9	Field Variables			
10	Temperature	Yes		
11	Shear Angle	No		
12	Degradation Factor	No		
13	Alternating Stress R-Ratio	Tabular		
17	Tensile Yield Strength	15	MPa	
18	Compressive Yield Strength	15	MPa	
19	Tensile Ultimate Strength	21.34	MPa	

**Figure 3.6.** Properties of material.

### 3.6.1.4 Meshing

The meshing process was done by choosing the volume and the number of elements in each body. The automatic size control (Automatic mesh) was used to mesh the model, as shown in figure (4.9). The number of elements (4644) for the model represents the specimen with the total number of (17698) nodes.

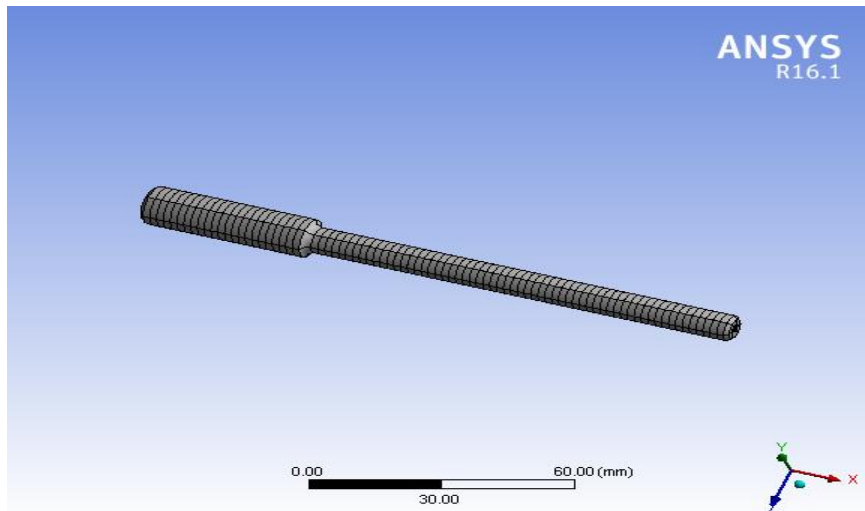


**Figure 3.7** Meshing.

### 3.6.1.5 Define the Analysis Type and boundary conditions

the boundary conditions were applied, such as supports and applied load. According to the model's geometry, in this work, the model was a cantilever beam where it was fixed from one end, and the load (10 N) apply at the other end, as shown in figure 3.8.

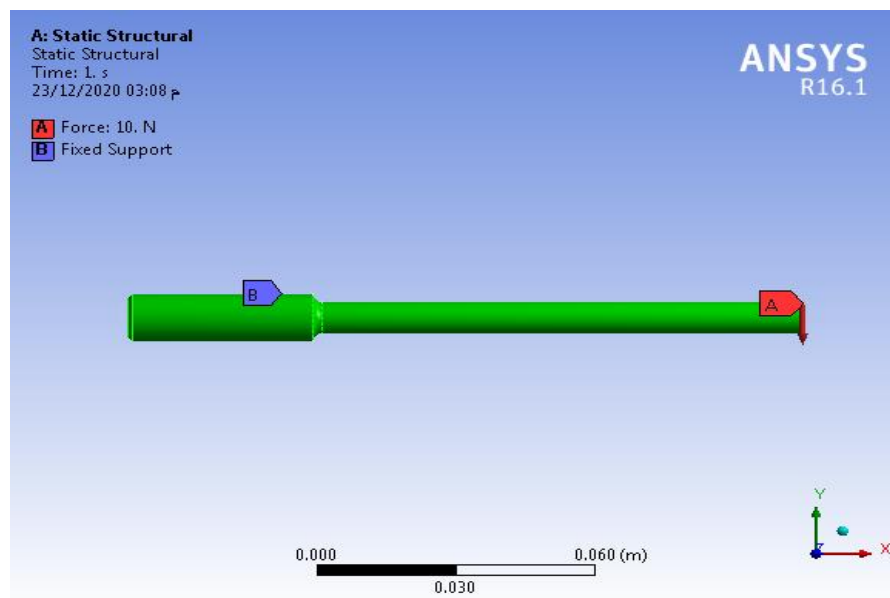


**Figure 3.8** The model and boundary condition.

After setting the boundary condition, the analysis and fatigue decision should be defined as fatigue analysis type, stress life . The next decision is whether to apply a mean stress correction.

### **3.6.1.6 Solution and results**

Generally, the results data taken out from the FEA solutions. The fatigue tool used in the solution of fatigue to find the equivalent stress, total deformation, damage, and life at different loads. The fatigue analysis used in the current work is based on a fully reversed bending ( $R = -1$ ).

# CHAPTER FOUR

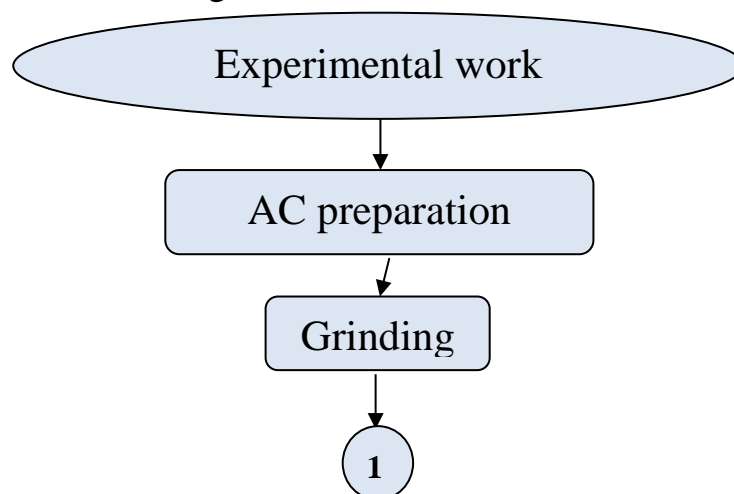
## Experimental Work

### 4.1 introduction

This chapter includes the details of the experimental work done, which was:

Fabricate the particulate epoxy composites in vacuum technique with different weight fraction ratios of AC (0, 5, 10, 15, 20, 25, 30, 35 and 40 wt. %) for tensile tests and (0,10,15,20%) wt. for fatigue tests with average particle sizes of about (14.74 $\mu$ m), which is measured during this work by Laser particle size analyzer. The Fourier Transform Infrared (FTIR) spectroscopy analysis was conducted to determine the interaction between AC particle and epoxy material. Differential Scanning Calorimeter (DSC) behavior of this biocomposite has been carried out to find the glass transition temperature ( $T_g$ ) of the pure epoxy and composites.

Tensile test and scanning electron microscopy (SEM) analysis were also performed to take some information about tensile strength and strength of an interaction between AC and matrix material. Finally, a fatigue test was accomplished to fatigue life for composites, all work procedures showing in the flow chart, as shown in figure 4.1.



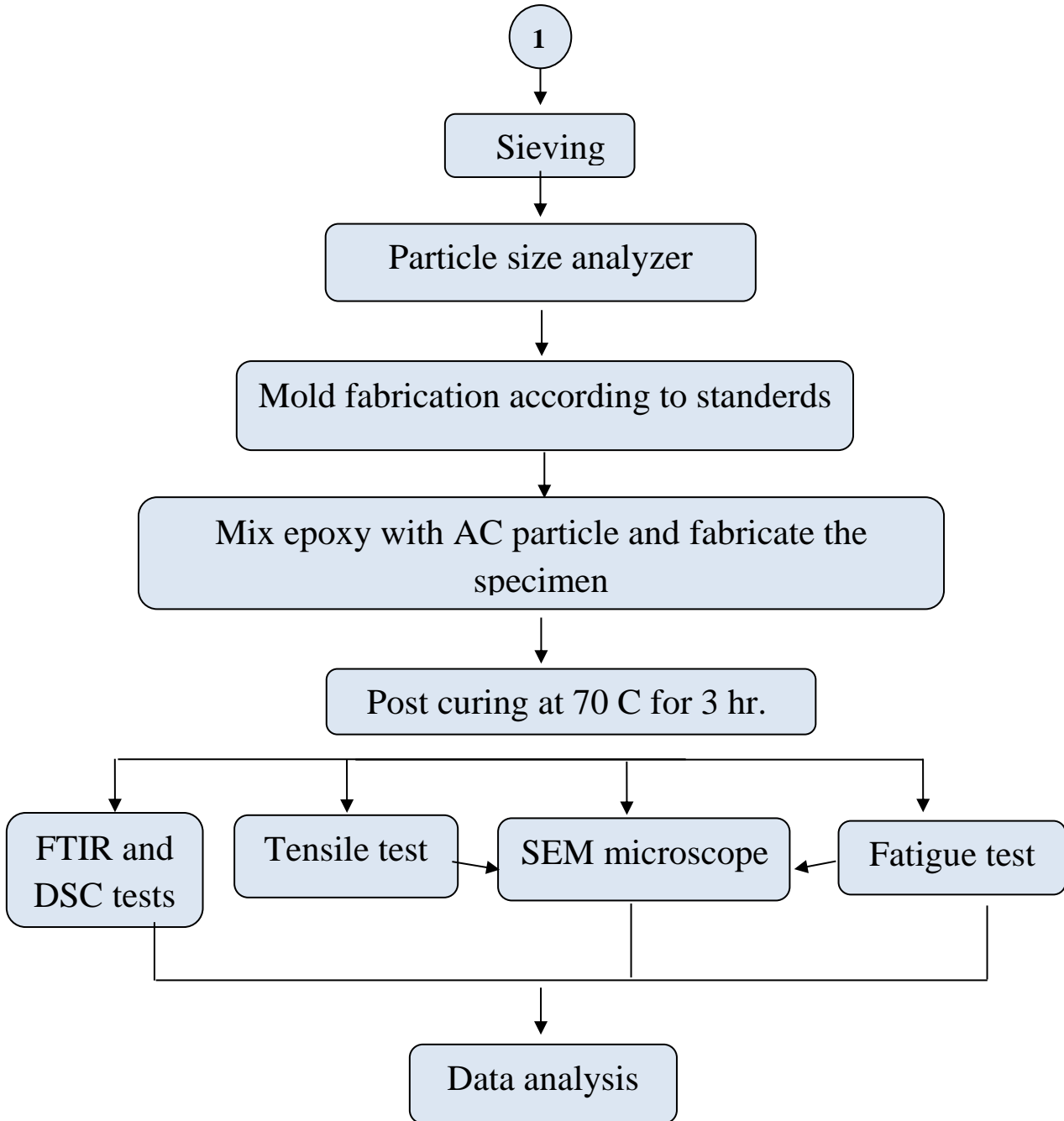


**Figure 4.1** Flow chart of the experimental work procedure.

## 4.2 Material

The epoxy resin used as matrix material provided from Sikadur 52 company, the epoxy resin (A) was mixed with the hardener (B) in the ratio of (2:1) by weight, the standard properties of epoxy resin were listed in table 4.1.

Activated carbon particles (figure 4.2) are used as reinforcement materials (from Shanxi Xinhui Activated Carbon Company, Ltd, Shanxi, China) with standard properties, as shown in table 4.2 . The purchased activated particles are grinding and sieving by standard sieves with size between (8-38)  $\mu\text{m}$ , the sieve put in a shaker in civil engineering laboratory in Babylon university , as shown in figure 4.3. Then the particles were analyzed by size analyzer device to obtain the average size of particles about 14.74 $\mu\text{m}$ , as resulted in chapter five, section 5.2.

**Table 4.1.** Standard properties of epoxy from company.

Property	Value
Tensile strength (MPa)	$\leq 25$
Flexural strength (MPa)	53
Modulus of elasticity (GPa)	1.060
Viscosity at 20 °C (mPa.s)	500
Density ( $\text{kg}/\text{m}^3$ )	1100



**Figure 4.2** Activated carbon particles.

Specification	Value	Definition
Iodine Number	950 min.	Measure of unsaturation of substance expressed as the number of grams of iodine absorbed by 100 gm of the substance .
Abrasion Number (ASTM):	90 min.	Measures the structural strength of granular activate carbon it is measure the ability of the particles to stand up to shear forces caused by particles rubbing together
Ash Content	5% max.	Measure the mineral oxide content of AC on a weight basis .
pH Range	6 - 8	Measure of whether AC it is acidic or basic .
Bulk Density (Kg/m <sup>3</sup> )	470 - 500	It is the mass of AC particles divided by the total volume they occupy .

**Table 4.2.** Standard properties of activated carbon particles from company.

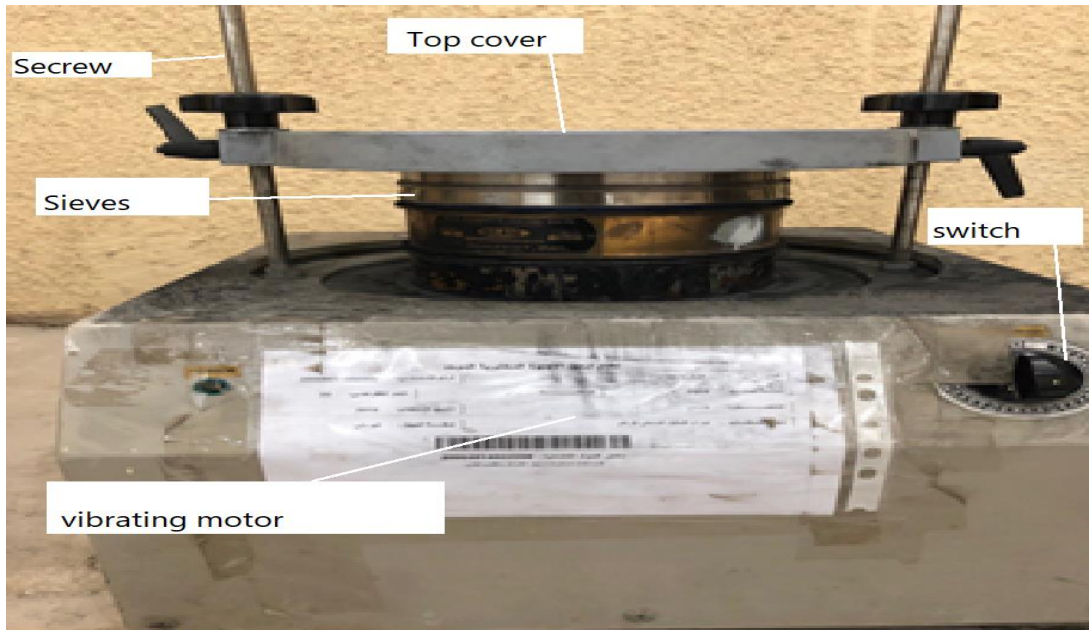


**Figure 4.3** Vibrating sieve

### **4.3 Composite fabrication**

Nine types of composites were fabricated during this work. The AC particles reinforced epoxy with different weight fraction ratios (0, 5, 10, 15, 20, 25, 30, 35, and 40%) for tensile tests and four types of composites (0,10,15,20%) for fatigue tests.

The AC particles were added to the epoxy resin and moved mechanically using a laboratory shear mixture at 1000 rpm for 1 h. During mixing, AC particles dispersed epoxy resin. For 30 min the mixture was left to release trapped air bubbles. A good-dispersed AC-epoxy combination with a stable suspension of the AC particles within the epoxy resin was obtained. To obtain the required composite samples, vacuum bag technology used, as shown in Figure 4.4. in mechanical engineering laboratory in university of Karbalaa , the mold of tensile specimen fabricated from PVC by CNC machine as shown in figure 4.5, for fatigue tests, the mold Fabricated from aluminum with two symmetrical pieces tied by the screw as shown in figure 4.6, the mixture of AC



particles with epoxy was poured into the mold. The mold was put inside a vacuum device for 24 hours to prevent air bubbles from the composite, where the pressure was reduced to lower than -30 psi, the composite specimens were left to dry at room temperature for 48 h. The product samples were left for 3 hours in an oven at 70°C to achieve sufficient curing, as shown in figure 4.7.

The resulting specimens shown in figure 4.8 and 4.9 .

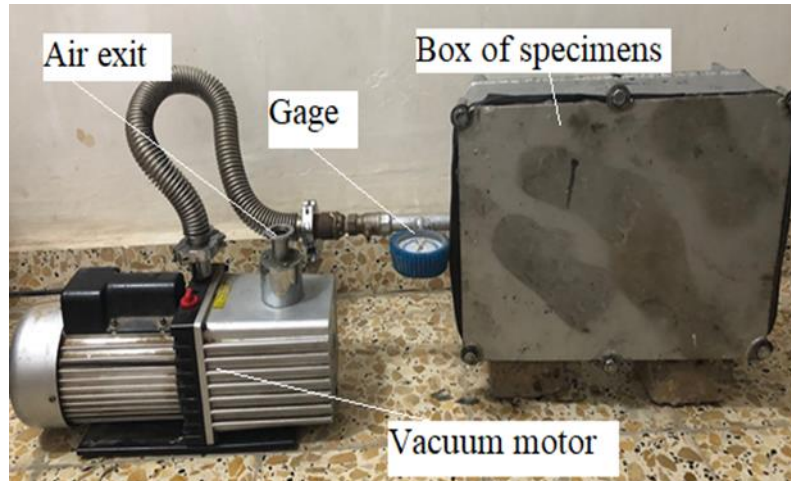


**Figure 4.4** Vacuum device



**Figure 4.5** Tensile mold.

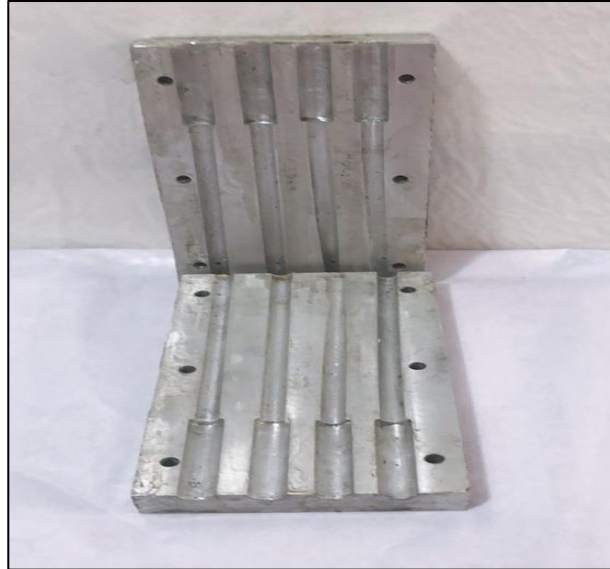


**Figure 4.6** Fatigue mold.



**Figure 4.7** Samples in the oven.



Figure 4.8 Tensile specimens.

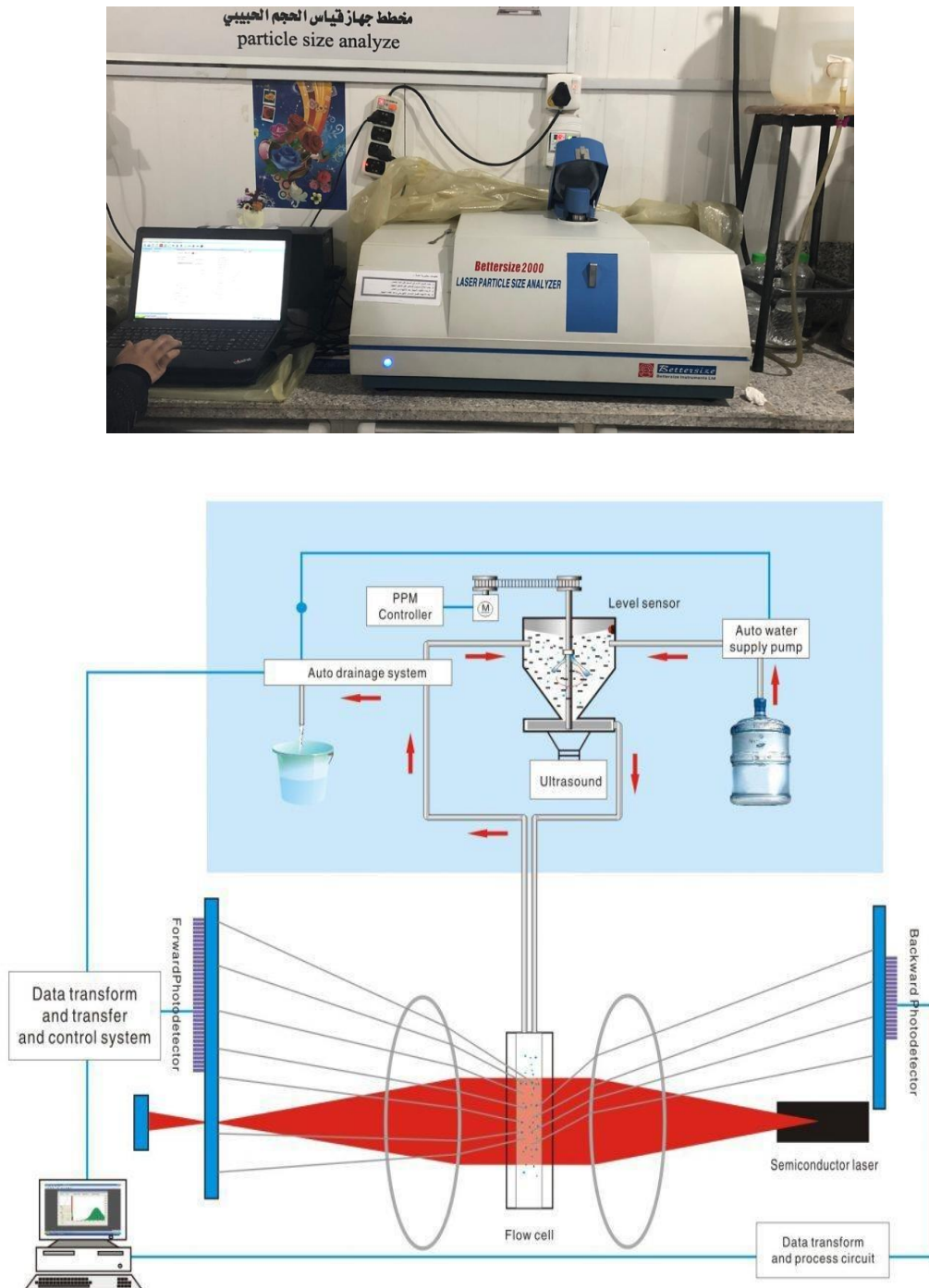


Figure 4.9 Fatigue specimens.

## 4.4 Experimental setup

### 4.4.1 Particle size analyzer

The Laser diffraction particle size analyzers device (Better size 2000, china), as shown in figure 4.10, was used to calculate particle size from the angle of light scattered by a stream of particles passing through a laser beam.



**Figure 4.10** Particle size analyzer.

### 4.4.2 Fourier transform infrared spectroscopy (FTIR)

FTIR is a technique used to analyze and identify materials (solid, liquid, and gas). FTIR analyses infrared light used to scan material samples to obtain the composite materials' chemical properties and physical bonding. The detector's resulting signal presents a spectrum from 4000 to 400 ( $1/\text{cm}$ ), representing a sample's molecular fingerprint.

The sample mix with potassium bromide (KBr) is used as a carrier for the sample because it does not show any absorption and transition 100% between 4000 to 400 ( $1/\text{cm}$ ).

FTIR used to know if the chemical structure remains the same between neat epoxy and epoxy composites (physical interaction). The samples scanned by IRAffinity-1 Fourier-transform infrared spectroscopy (FTIR) Shimadzu, shown in figure 4.11.

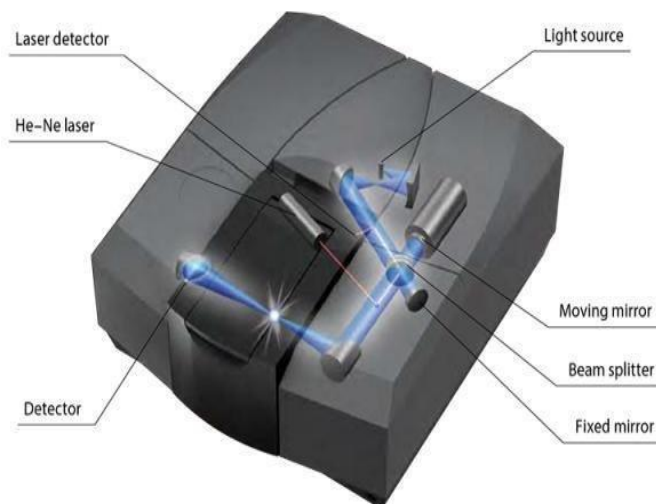


**Figure 4.11** Fourier-transform infrared spectroscopy (FTIR)

### 4.4.3 Differential scanning calorimetry (DSC)

Differential scanning calorimetry (DSC-60) SHIMADZO, shown in figure 4.12, was used. It is a thermal analysis technique that measures the rate of heat flow and compares the test sample's heat flow rate and known reference materials as a function of temperature.

The difference determines variations in material composition. These variations showed in curves. It is a very powerful technique to evaluate material properties such as glass transition temperature, melting, crystallization,

specific heat capacity, cure process, purity, oxidation behavior, and thermal stability.

The sample must be a suitable size and shape to fit in the small aluminum pan, as shown in figure4. then it put in the device for 15 minutes; meanwhile, a curve appears on the screen .

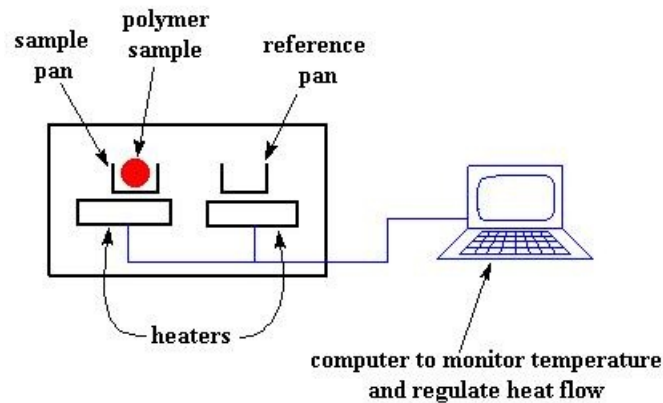


**Figure 4.12** Differential scanning calorimetry (DSC).

#### 4.4.4 Tensile test

According to the ASTM D638 [38] specifications, the tensile specimens were performed using the universal testing machine of type H50KT-0404, Tinius Olsen, UK, shown in figure 4.13, with a cross-head speed of 2 mm/min with load range 50 N, for more accuracy, three specimens for each composite has been tested, and the average value of each weight fraction was taken.

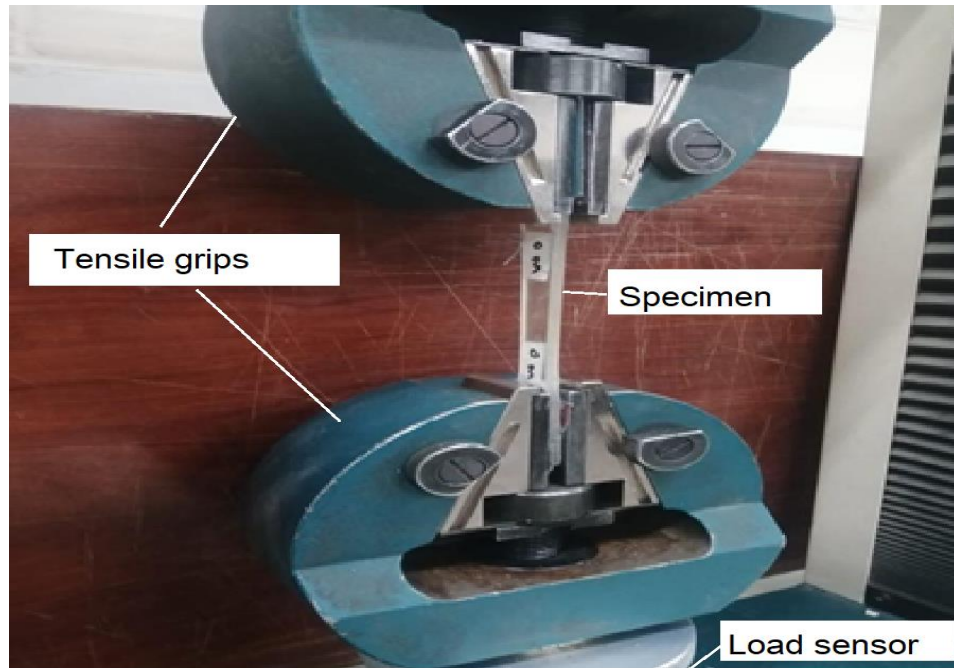


**Figure 4.13** Universal tensile testing machines type H50KT-0404, Tinius Olsen, UK.

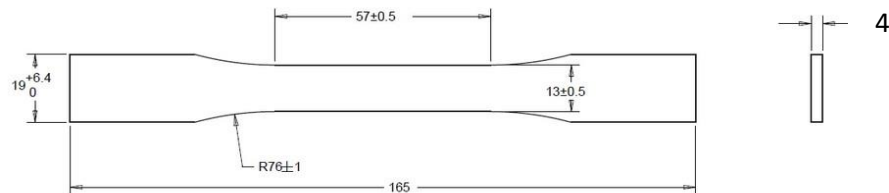


**Figure 4.14** Tensile specimen according to the specification of ASTM 638. (dimension in mm)

#### 4.4.5 Fatigue test

According to ASTM WP-140[39] specifications, fatigue test specimens were performed using the fatigue test machine, a machine accomplished by the company.



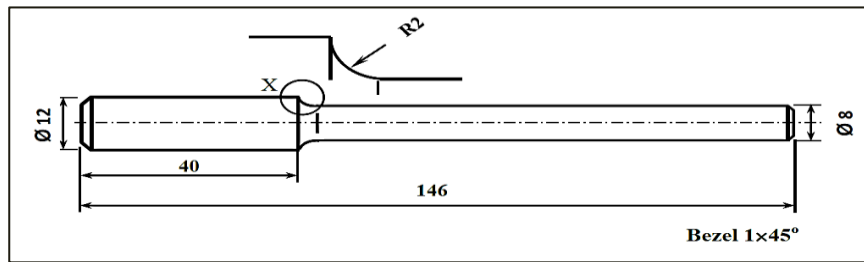


**Figure 4.15** Fatigue test specimens according to ASTM WP-140 specifications [39] (all dimension in mm).

The specimen is subjected to a pure reversed bending stress in the machine figure 4.16 and loaded with a concentrated force ratio of  $R = -1$ . The load  $F$  is applied on the opposite side perpendicular to the specimen's axis to obtain the rotating bending fatigue conditions. The experiment is conducted by repeating many similar procedure tests for all the specimens by varying the applied load at each trial and counted the cycle number to failure, and draw the S-N curve for the recorded data., Bending moment values are used to determine the alternating bending stress, which can be resolved directly from the equation.

The bending moment is calculated with the load and the lever arm as follows

$$M = F \cdot a \quad (4.1)$$

By using the section modulus of the specimen, it is possible to calculate the alternating stress amplitude:

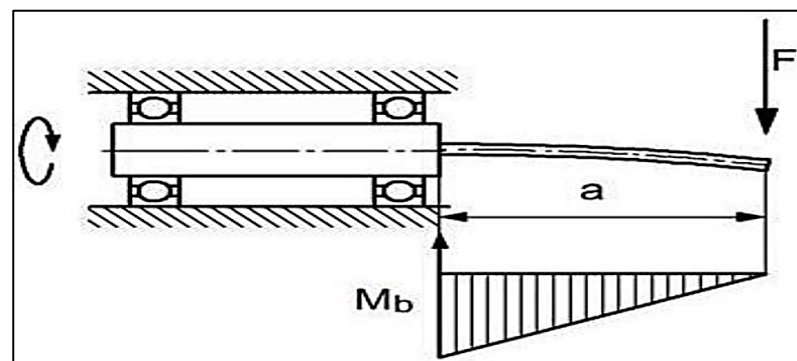


**Figure 4.16** The load on a clamped specimen [40]

$$\sigma = \frac{M}{W} \quad (4.1)$$

$$W = \frac{\pi d^3}{32} \quad (4.2)$$

$$\sigma = \frac{32 F.a}{\pi d^3} \quad (4.3)$$

$\sigma$ : Maximum alternating stress (MPa).

F: Applied load (N).

a: Bending arm =106 mm.

d: Diameter of the specimen =8 mm.

M: Bending moment (N.mm).

W: Section modulus of the specimen( $m^3$ )

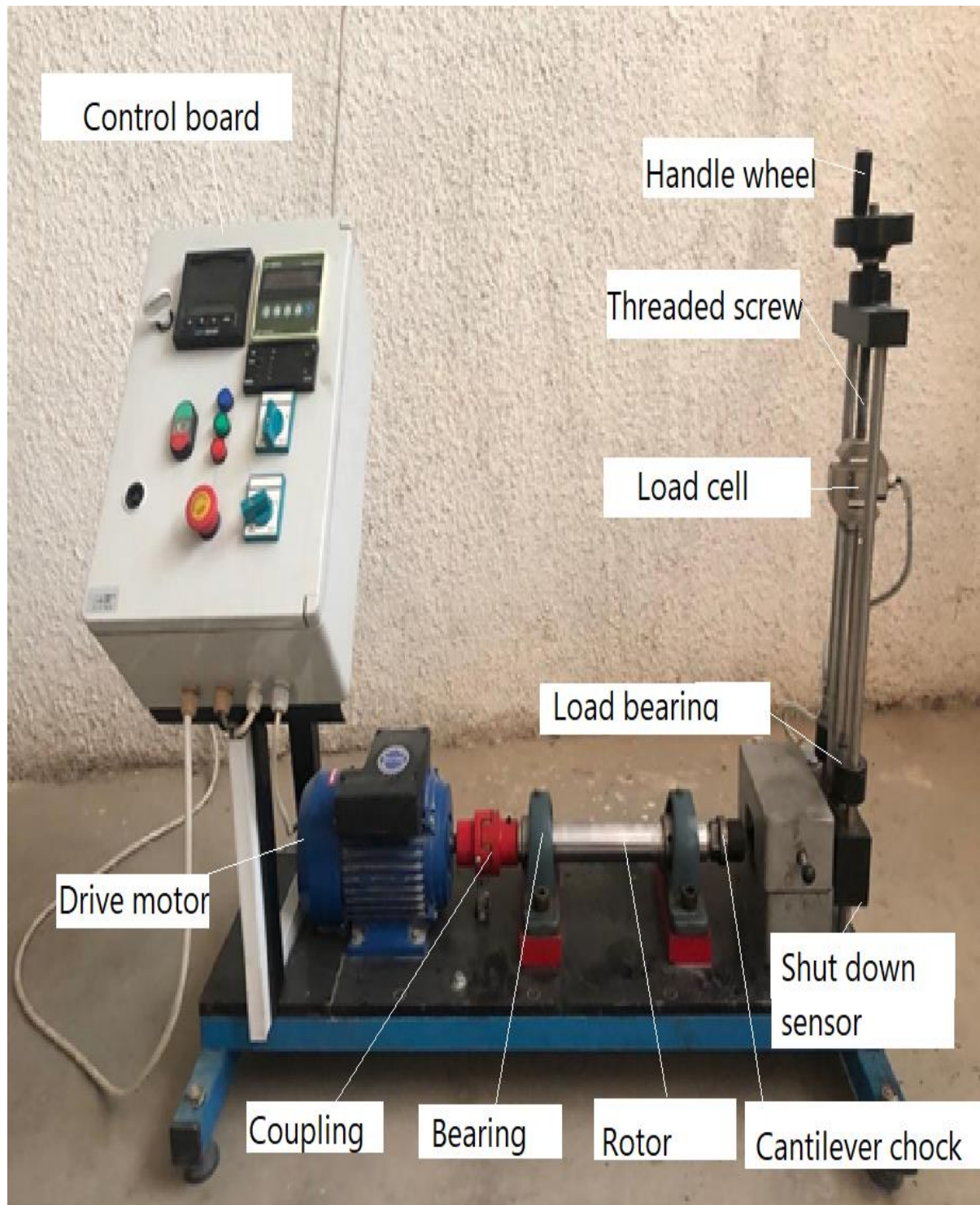
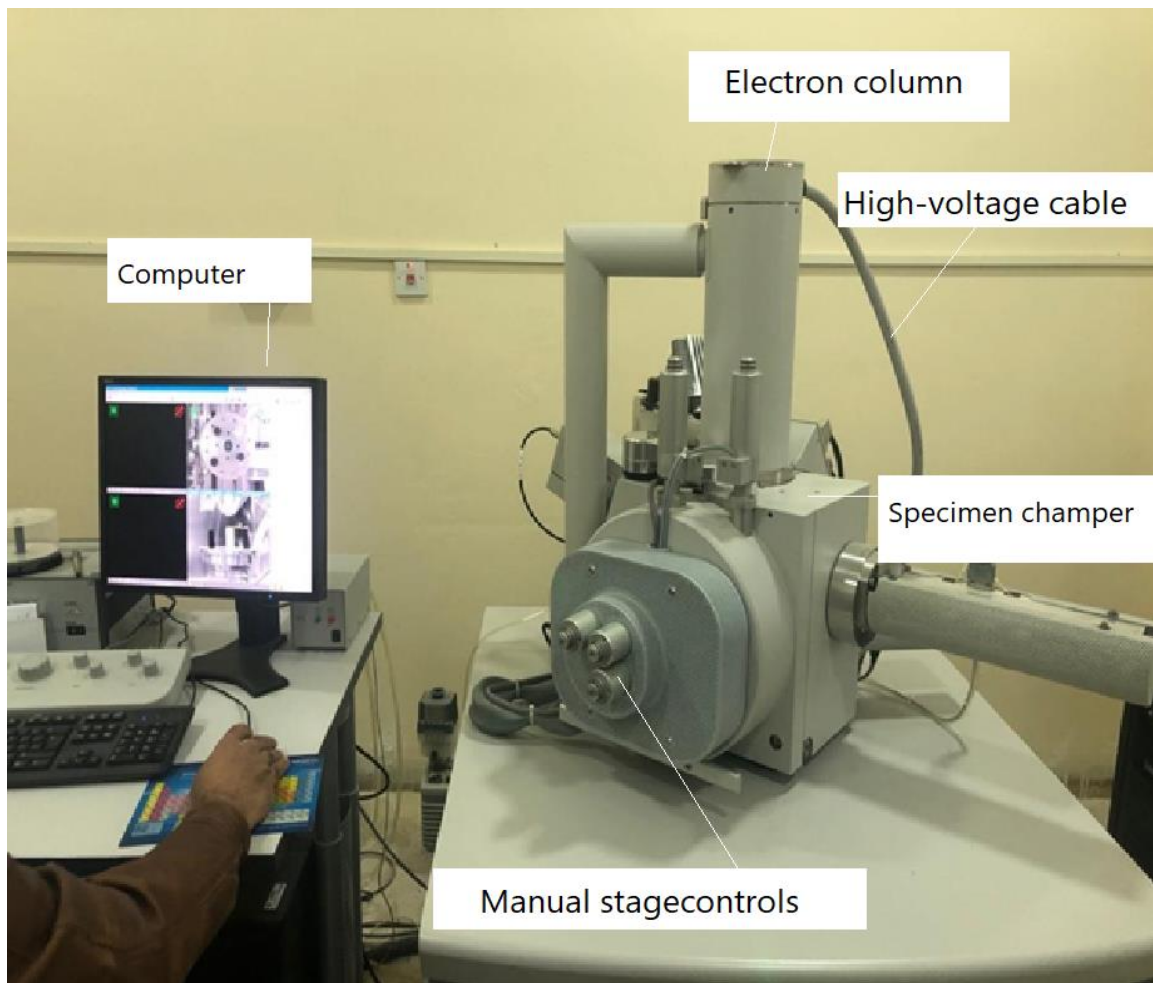


Figure 4.17 Fatigue machine.

#### 4.4.6 Scanning electron microscope (SEM)

Microstructures of the composites were assessed with scanning electron microscopy. FEI Quanta 450 scanning electron microscope (USA), shown in figure 4.18, was used to exam the prepared composites specimens to show the nature of fracture of tensile and fatigue specimens.



**Figure 4.18** Scanning electron microscope (SEM).

# CHAPTER FIVE

## Results and Discussion

### 5.1 Introduction

In the current chapter, the results obtained experimentally and numerically are recorded and investigated for epoxy/AC particles composite with different weight fraction of AC particles, several experimental results obtained from the particle size analyzer, Differential Scanning Calorimeter DSC, Fourier Transform Infrared FTIR, tensile, fatigue and Scanning Electron Microscopy SEM.

The numerical results are obtained using ANSYS workbench software program version 16 in the modeling of fatigue to compare with the experimental results and get the information about safety factor and the relationship between fatigue life and alternating stress stress ratio  $R=-1$ .

### 5.2 Particles measurement

Particle size distribution analyses a specimen with different size ranges and gives the number of particles of several sizes are present in the specimen, as shown in figure 5.1.

Distribution of particle size D50 is defined as an average value of particle size distribution, which is particles size at 50% in cumulative distribution . The particle diameter of the AC powder was measured during this work. It was found that; D10 =2.945  $\mu\text{m}$  means a cumulative 10% point of size, D50 =14.74  $\mu\text{m}$  is also defined as average particle diameter, and D90 =28.7  $\mu\text{m}$ .

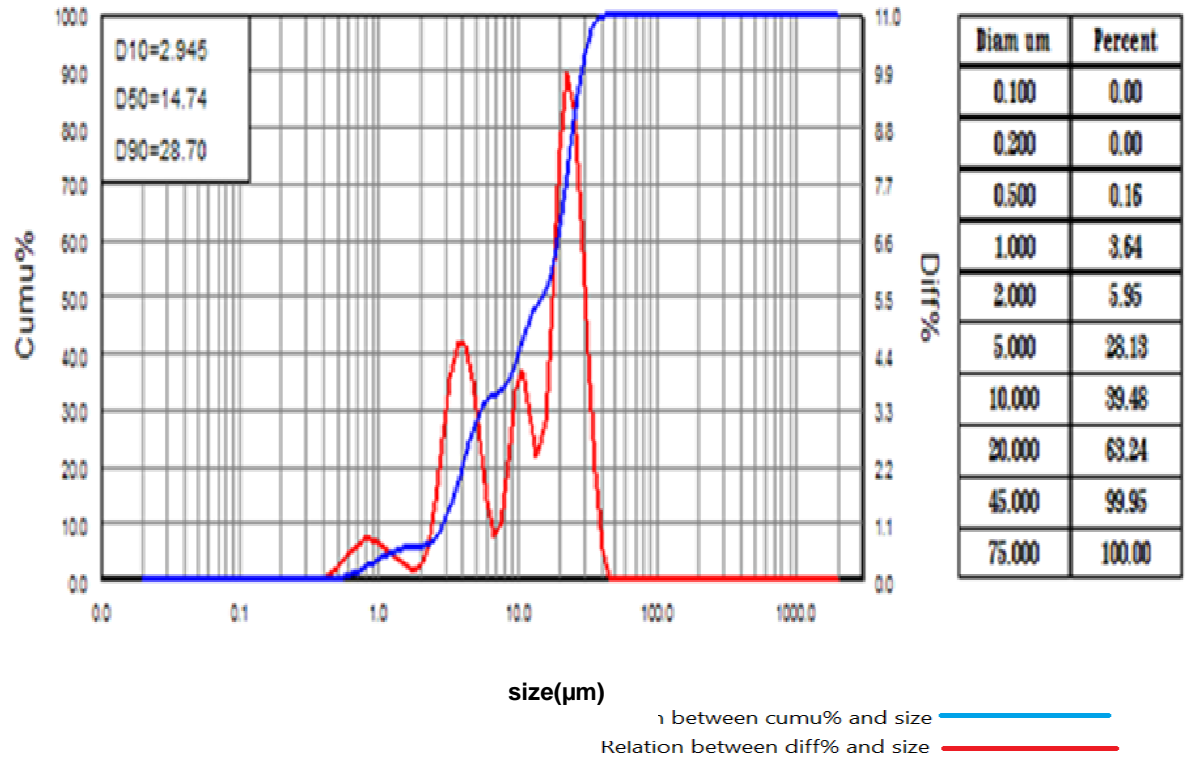


**Figure 5.1** Size distribution of AC particles.

### 5.3 Fourier-transform infrared spectroscopy (FTIR) results

Figure 5.2 shows the results of FTIR test, which done between 4000 (1/cm) & 400 (1/cm) wave length, the functional group that appeared for pure epoxy was: OH, appear at wave number 3433.29 (1/cm) [41] [42], the band at 2925.58 (1/cm) is characterizing to CH<sub>2</sub>[49], the band at 2870.08 (1/cm) gave CH<sub>3</sub> [43], at 1612.49(1/cm) assigned C=O, at 1512.19 (1/cm) and 825.53(1/cm) assigned aromatic bonds [41][42], at 1242.16 (1/cm) and 1033.85 (1/cm) indicate C-O-O ether bonds [42].

The FTIR results of pure epoxy and epoxy composites (0,5, 10, 15, 20, 25, 30, 35 and 40%) are clarified in figure 5.2; it can be noticed that there are no new peaks appeared after reinforcing by the AC powder; also, there was

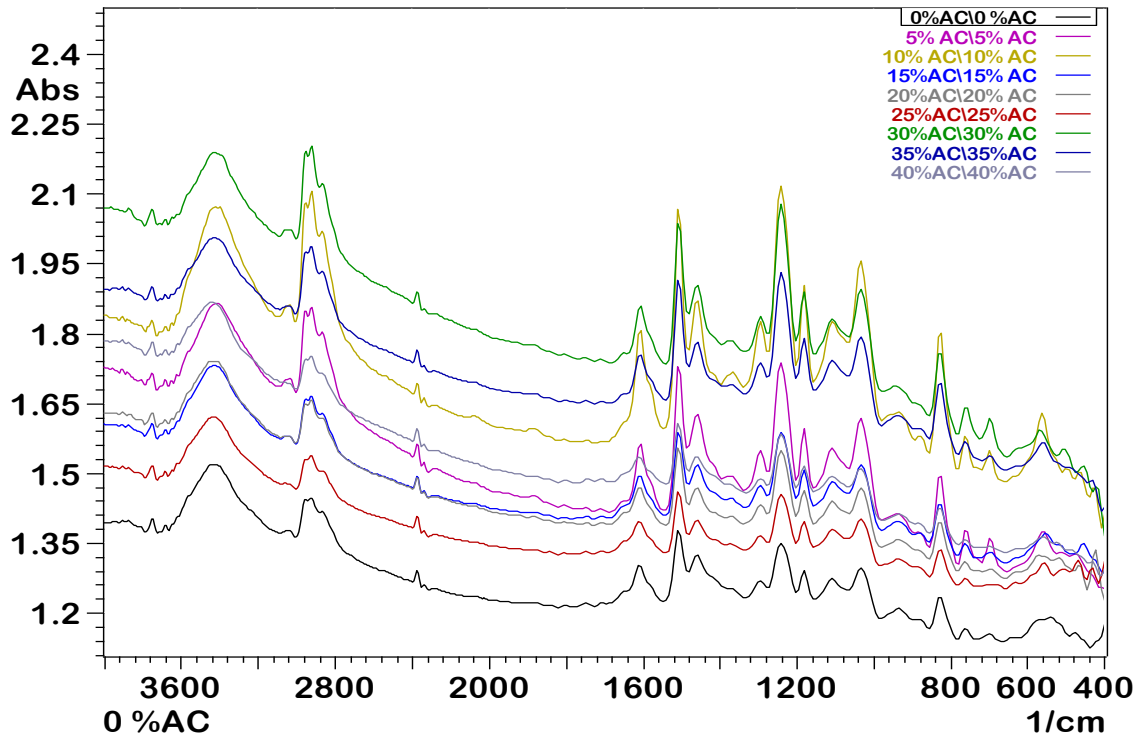


**Figure 5.2.** FTIR spectra of all specimens, where the x-axis represent wavelength in (1/cm) and the y-axis represent the absorbance (Abs).

no shifting in any of these peaks, the absorbance of the all-composite peaks increased with the increase in the concentration of AC particles, this behavior refers to find Physical bonds composite constituents; this is giving a good indication of improvement the miscibility state between composite constituents, and absence any residual monomer.

## 5.4 Results of Differential scanning calorimetry (DSC)

The glass transition temperatures ( $T_g$ ) of neat epoxy and epoxy/activated carbon composites are calculated by differential scanning calorimeter (DSC).

$T_g$  is an essential factor in composites and epoxy resins that defines the temperature of applications. It is normally below  $T_g$ .

It was determined for each specimen from the midpoint of the corresponding glass transition regions. As shown in curves in Appendix A. Table 5.1 shows glass transition temperature for neat epoxy and epoxy reinforced with (5, 10, 15, 20, 25, 30, 35, 40) % wt. Activated carbon. From this analysis, it can be indicated that  $T_g$  of the composite specimens increased continuously with increased weight fraction ratios of activated carbon. It is observed from this table that the neat epoxy has  $T_g$  of 147.76 °C, agrees with [43], and the highest value obtained in 40%wt. Which increased by 30.5% as compared with neat epoxy.

The increase in the  $T_g$  AC addition may be attributed to high cross-link strong interfacial between the particles and epoxy, which reduces the chains' mobility around the high surface area microporous particles. Finally, the increase in the crosslink density may result in higher  $T_g$  [44],[45].

**Table 5.1** Glass transition temperature for neat epoxy and epoxy composite.



AC % wt.	T <sub>g</sub> (°C)	Increased by %
0%	147.76	0
5%	151.39	2.4
10%	162.13	7.09
15%	177.48	9.4
20%	177.50	0.011
25%	179	0.84
30%	186.8	4.4
35%	190.11	1.77
40%	192.83	1.43

### 5.5 Tensile test result

Figures 5.3 and Table 5.2 shows the results of tensile properties of neat epoxy and epoxy reinforced activated carbon powder specimens with (0,5, 10, 15, 20, 25, 30, 35, 40) % wt. fractions, 3 specimens for every weight fraction, and the nonlinear behavior of all samples are obtained.

The ultimate tensile stress increases with increasing of activated carbon particles weight fraction until reaching the maximum value at 15%, which was 26.34 MPa (18.87%), because of the high connection between epoxy and activated carbon particles due to a high surface area of this particle with addition the adhesion of epoxy is excellent after that, the ultimate tensile stress begins to decrease to reach the lowest value at 40%, which was 18.15 MPa

decreases by about (30.99%) as compared with neat epoxy as shown in figure 5.4; this is attributed to the debonding between AC Particles and epoxy matrix and the number of agglomerations is increasing and becomes more present as a result of the increasing of AC content where it acts as a stress concentration, and this contributes to decreasing strength.

The increased loading of AC to 15 % wt led to an increase in the tensile modulus of the composite to the max value of 2.902 GPa due to the addition of AC particles which impart stiffness. After 15 % wt. of activated carbon loading, deterioration occurred in the material's tensile modulus. This is due to the increasing brittleness of composite due to the AC particle brittleness nature.

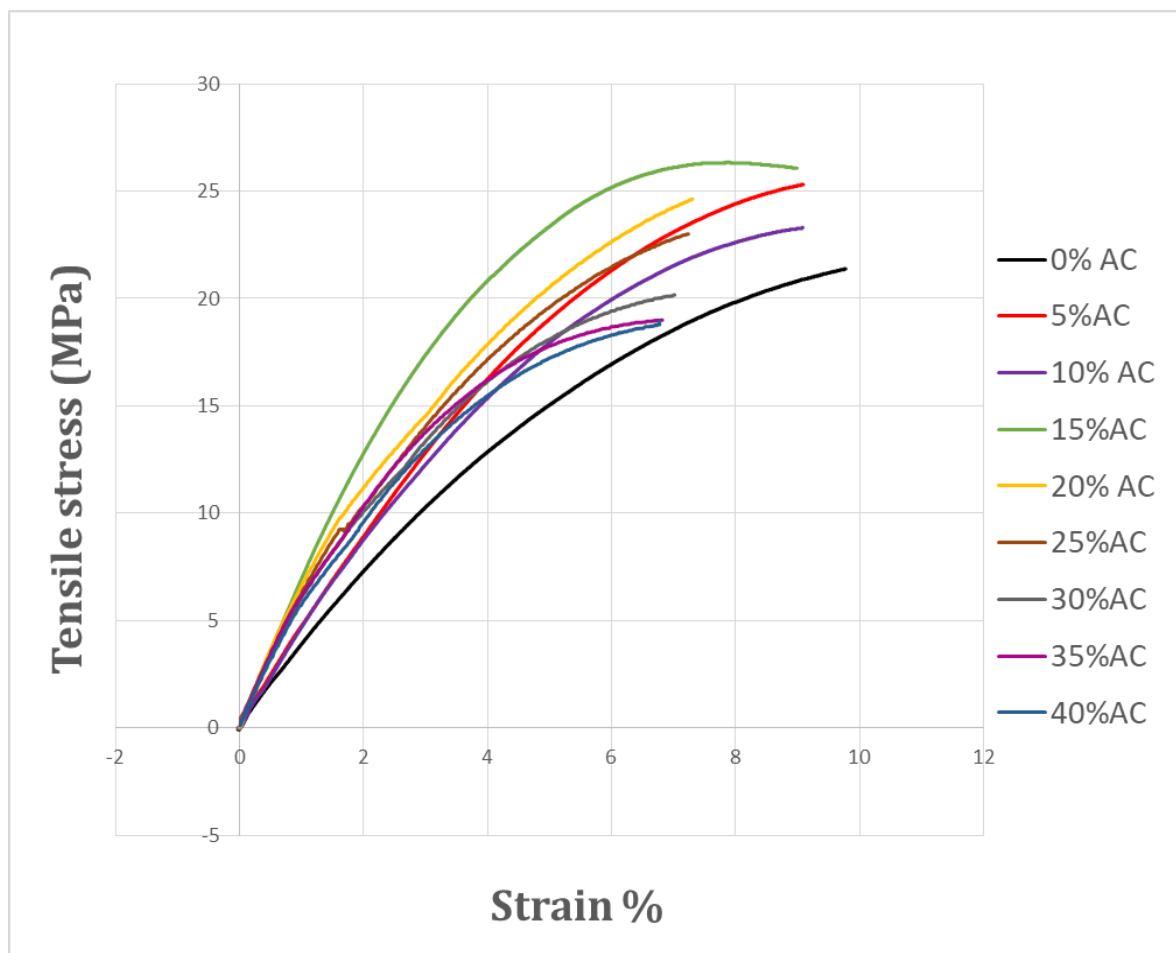
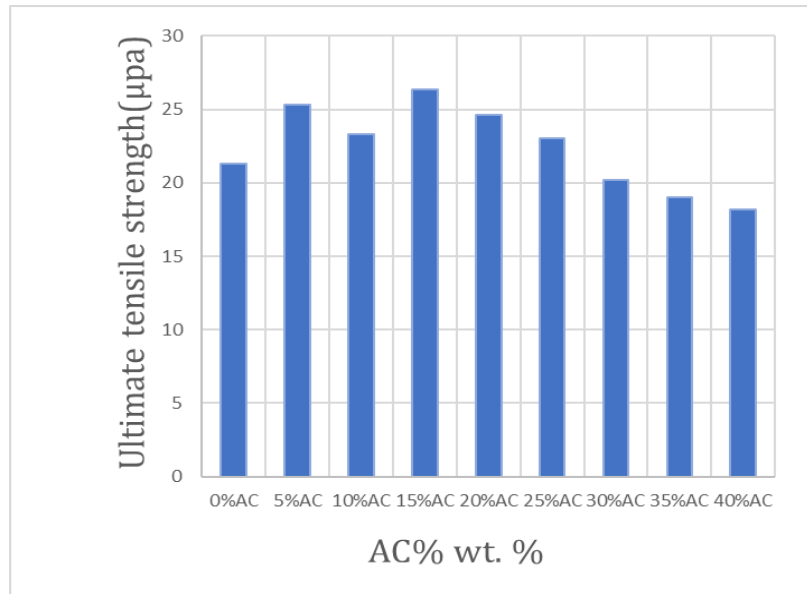
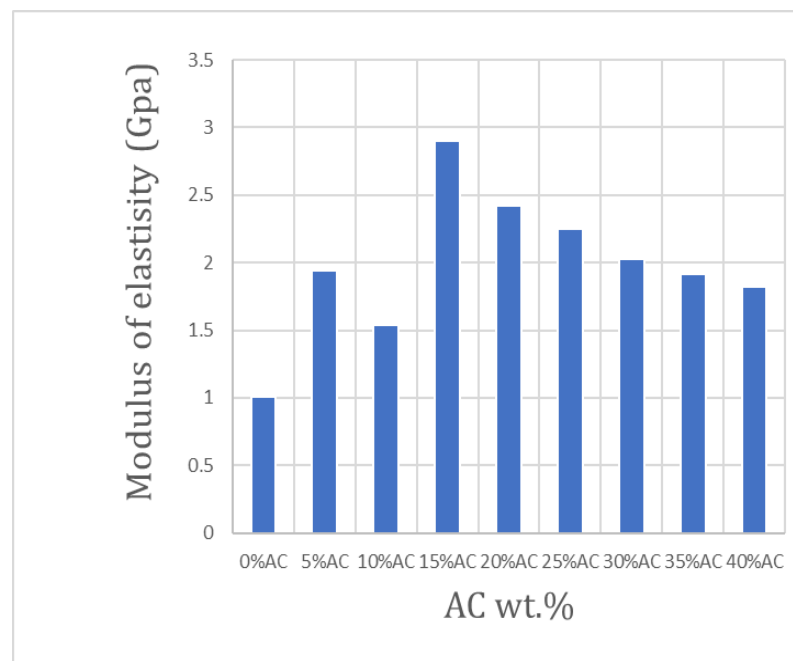


**Figure 5.3.** Stress-strain diagram for pure epoxy and its composites.



(a) The effect of activated carbon content on ultimate tensile strength.



(b)

(b) The effect of activated carbon content on the modulus of elasticity.

**Figure 5.4 (a) and (b)** The relation between ultimate tensile strength, modulus of elasticity with AC % content

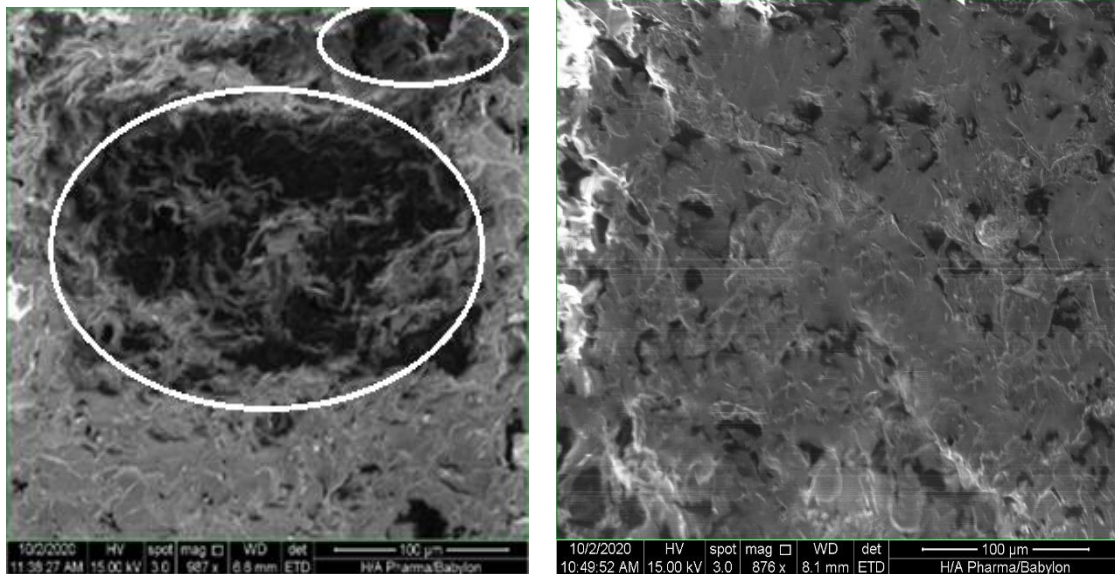
**Table 5.2** The effect of activated carbon % wt. on tensile tests.

Activated carbon % wt.	Ultimate tensile strength $\sigma_{ult}$ (MPa)	Yield stress $\sigma_y$ (MPa)	Modulus of elasticity E (GPa)	Strain at breakpoint %	Poisson ratio	Improvement in $\sigma_{ult}$ (%)	Improvement in E(%)
0%	21.34	15	1.01	9.77	0.34	0	0
5%	25.3	18	1.945	9.5	0.3	18.5	92.5
10%	23.304	17	1.539	9	0.3	-7.88	-20.8
15%	26.34	19	2.902	8.97	0.32	13.02	88.56
20%	24.6	15	2.42	7.3	0.31	-6.6	-16.6
25%	23.004	14	2.254	7.24	0.3	-6.4	-6.85
30%	20.16	13.41	2.030	7.03	0.3	-12.36	-9.12
35%	19	13	1.919	6.99	0.32	-5.75	-5.46
40%	18.15	12	1.818	6.82	0.3	-4.4	-5.26

## 5.6 Results of the Scanning electron microscope (SEM) of fractured surfaces of tensile specimens

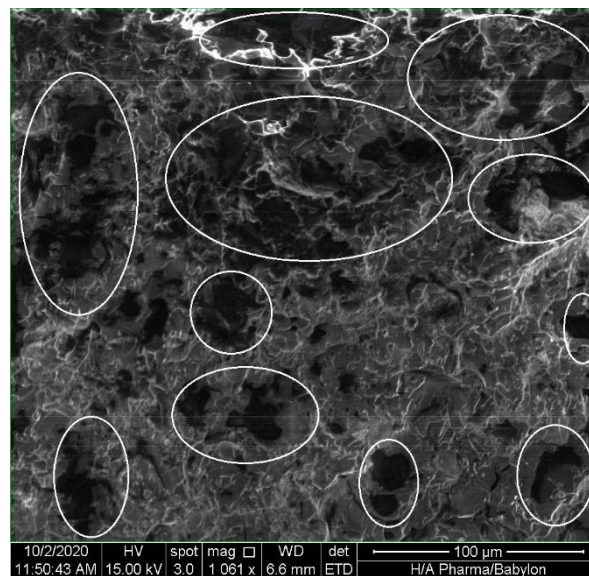
Scanning electron microscope (SEM) micrograph shows the fracture surface and a morphological inspection to investigate the microstructure of tensile specimens of activated carbon filled epoxy composites with 10, 15 and 20 % wt. as can be seen in figure 5.5 (a, b, and c respectively). The SEM test was conducted to examine the effect of activated carbon powder loading and the adhesion of particles–matrix interphase of the composites, and activated carbon particles' distribution in the matrix.

The composite failed by the brittle way, as shown in Figure 5.5, the micrograph of 10 % wt., the micrograph shows agglomeration and inhomogeneous distribution of activated carbon powder, which specified by elliptic white color; this is due to the bad mixing, as shown in figure 5.5 (a); in contrast, the mixing seems better distribution in 15 % wt. as shown in figure 5.5 (b), the micrograph of 20 % wt., seen in figure 5.5 (c), shows there is a de-bonding or detached phenomenon between the activated carbon powder and epoxy matrix moreover, the numbers of carbon clusters are increased due to the increase in carbon powder content which is act as stress concentration regions lead to decrease the strength of the composites.



(a)

(b)



(c)

**Figure 5.5.** Micrographs by Scanning electron microscope (SEM) images of fracture surfaces of tensile specimens for (a) 10 % wt. of activated carbon (b) 15 % wt. of activated carbon (c) 20 % wt. of activated carbon.

## 5.7 Results of Fatigue Tests

The factors affecting fatigue in the particulate composite are many, such as the type of material, the shape of the part, the weight fraction of particles, the size of particles, the material of matrix and particles, the dispersion of particles, and the stress ratio (R).

### 5.7.1 Experimental results

The fatigue tests were carried out for the composites with weight fraction (0,10,15,20%), 7 specimens for each weight fraction are used in this test (the total number 28 specimens), with stress ratio  $R=-1$ , where a series of tests have proceeded with different applied moments. The number of cycles to failure was counted. This procedure is repeated to the other specimens at progressively decreasing the applied stress amplitude. The results recorded are displayed graphically in the form of S-N curves, as shown in figure 5.6, which show the S-N curve of epoxy reinforced with (0,10,15,20%) wt. fraction of activated carbon particles.

The power-law equations and their constants which express the fatigue behavior of the composite materials and their correlation coefficient ( $R^2$ ) are given in table 5.4. The equations have a high correlation factor that indicates the experimental data well explained by the power-law formula. Since the correlation coefficient is a hand measure of the goodness of fit.

In the first instant of the results shown in figure 5.6, the fatigue strength decreases with increasing the number of cycles until failure. It quickly reduced in the first hundred thousand cycles. This is the first region in which the fatigue life initiates the first damages. As cycles increase, the decrease in the stress takes a new pattern, and the reduction is less sharp and starts to take near-linear decreasing and could be seen as a slope between two points to the final failure at the end  $10^6$  cycles.

From S-N curves shown in figure 5.6, the fatigue strength increases with the increasing of particles weight fraction until 15 % by 18.18%, then decreased at 20% by 5.45% because of agglomeration and that proportional to tensile strength [46], the endurance limit of the tested material is taken several cycles of  $10^6$  .

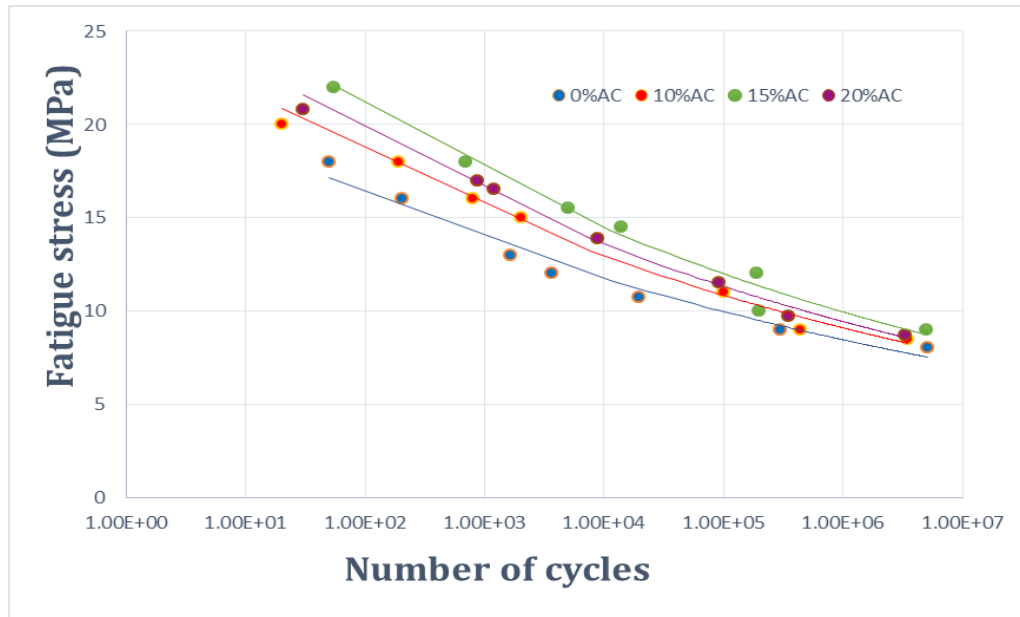


**Figure 5.6** Experimental S-N curves of epoxy composite reinforced with activated carbon particles with weight ratio (0,10,15,20%).

**Table 5.4** Experimental S-N curves equations (Basquin's equation) and correlation coefficient for (0,10,15,20%) wt. of activated carbon particles.

AC wt. fraction	Basquins equation	Correlation coefficient $R^2$
0%	$\sigma=22.546N^{-0.07}$	0.9708
10%	$\sigma =26.39N^{-0.075}$	0.9991
15%	$\sigma =30.205N^{-0.08}$	0.9656
20%	$\sigma=27.9.82N^{-0.079}$	0.9899



### 5.7.2 Numerical results

ANSYS workbench 16 software packages were used to simulate the experimental fatigue test for the same weight fraction (0,10,15,20%) wt. fraction, also to know the safety factor, fatigue life and Von-Mises stress.

Constant amplitude loading as a fully reversed (stress ratio  $R = -1$ ) used, a specific cyclic load applied to find the amount of equivalent alternating stress resulting in the sample due to this load and number of cycles as shown in figure 5.7.

Table 5.5 displays the numerical S-N equation (Basquin's Equation). As mentioned in equation (18) in chapter three, Basquin's equation was used for curve fitting. The constants of Basquin's equation and correlation factors are given in Table 5.5.

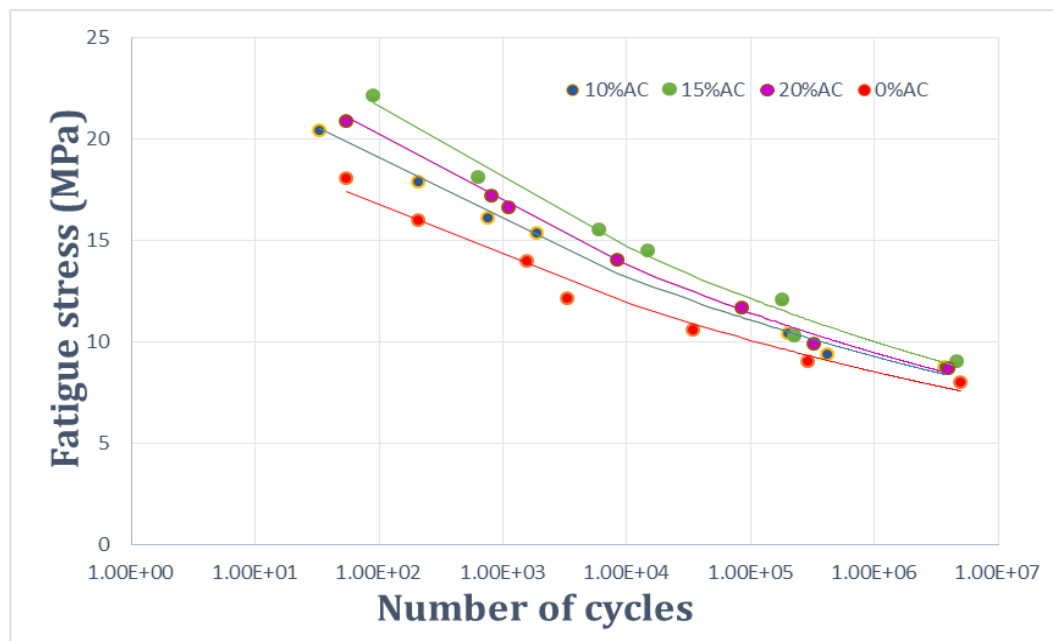


**Figure 5.7** Numerical S-N curves of epoxy composite reinforced with activated carbon particles with weight ratio (0,10,15,20%).

**Table 5.5** Numerical S-N curves equations (Basquin's equation) and correlation coefficient for (0,10,15,20%) wt. of activated carbon particles.

AC fraction	wt.	Basquin's equation	Correlation coefficient $R^2$
0%		$\sigma = 23.262N^{-0.072}$	0.981
10%		$\sigma = 27.615N^{-0.081}$	0.9936
15%		$\sigma = 31.157N^{-0.082}$	0.9821
20%		$\sigma = 28.373N^{-0.079}$	0.9957

### 5.7.3 Comparison between experimental and numerical results

Figure 5.8,5.9,5.10,5.11 shows the comparison between numerical and experimental which shows a good agreement between them with a maximum difference of about 4.43%

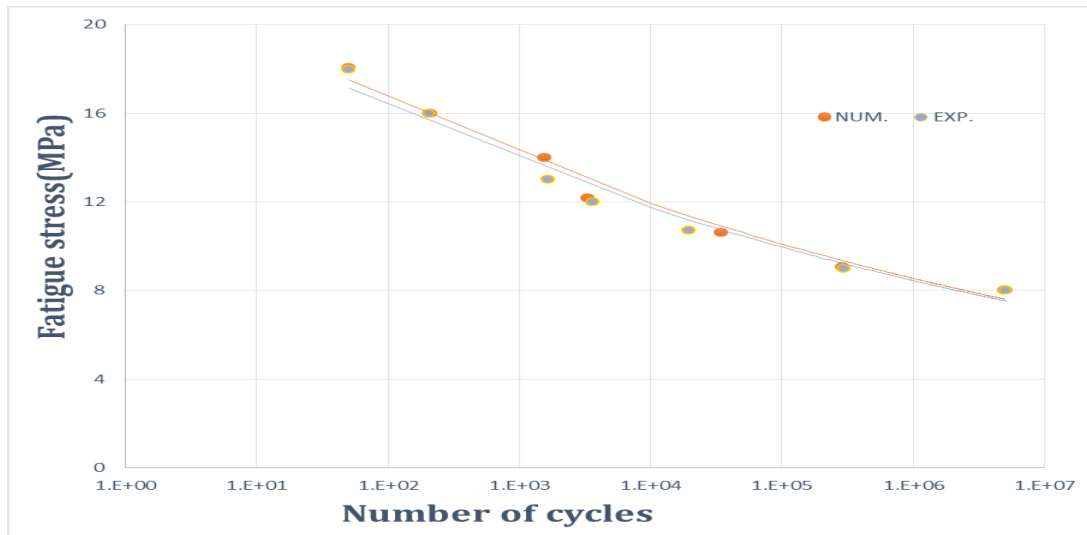


**Figure 5.8** Comparison between experimental and numerical S-N curve for 0% wt. fraction.

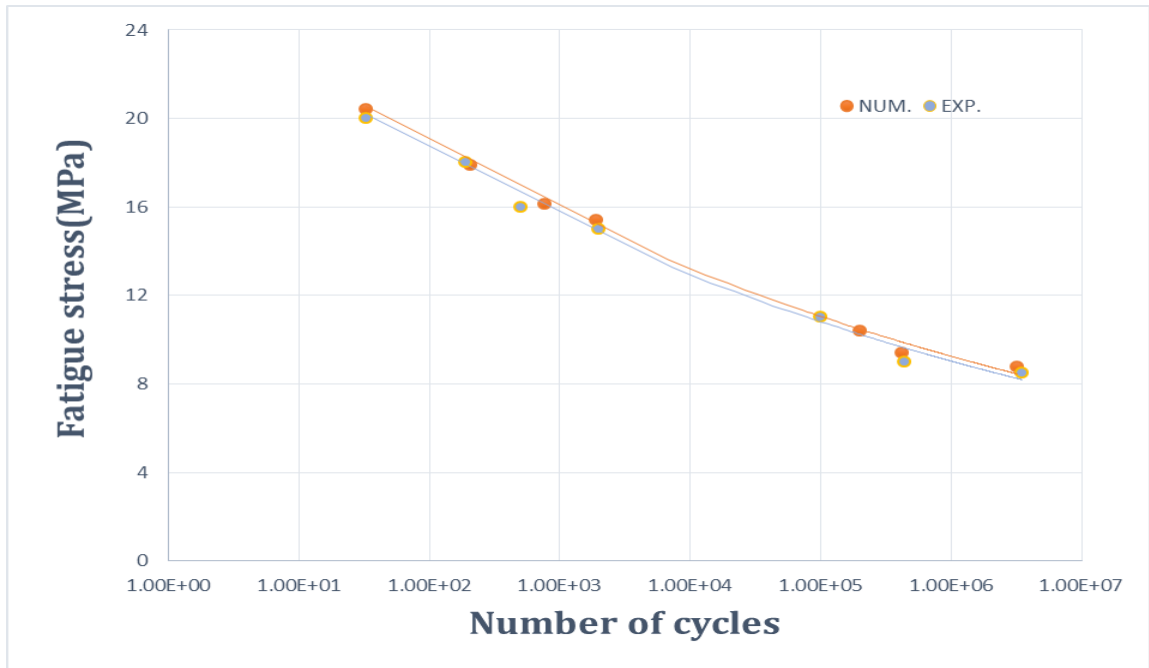


**Figure 5.9** Comparison between experimental and numerical S-N curve for 10% wt. fraction.

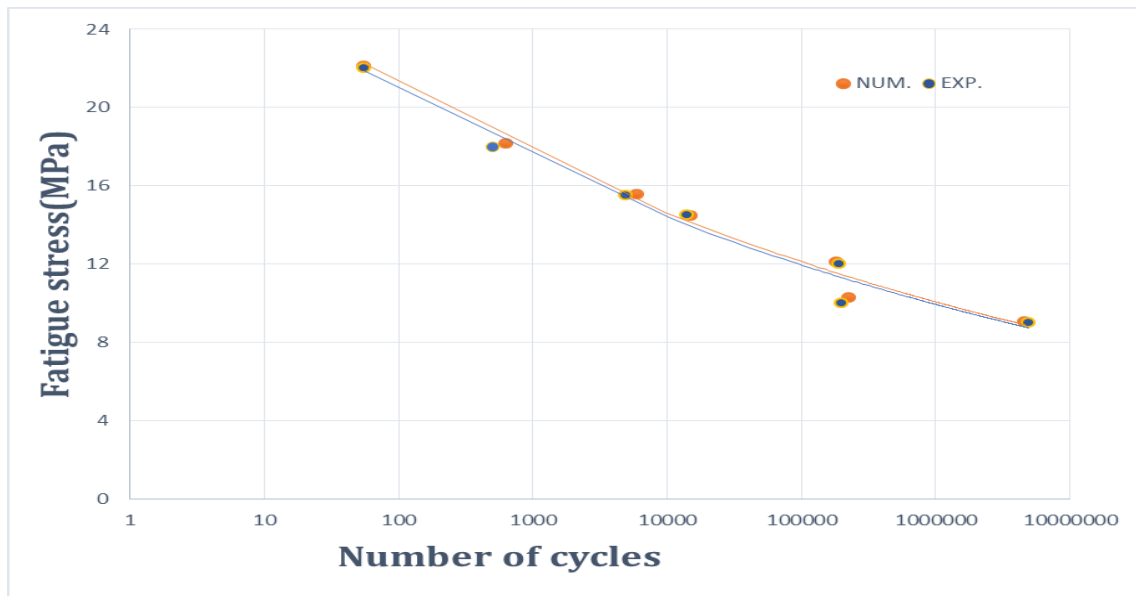


**Figure 5.10** Comparison between experimental and numerical S-N curve for 15% wt. fraction.

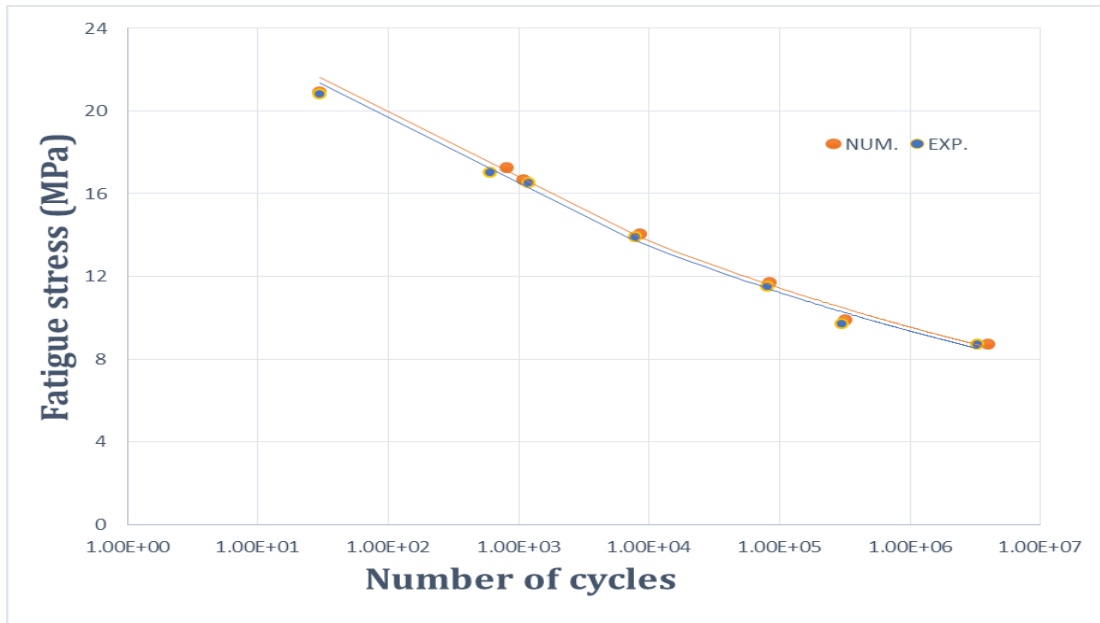


**Figure 5.11** Comparison between experimental and numerical S-N curve for 20% wt. fraction.

#### 5.7.4 Contour plot by ANSYS workbench

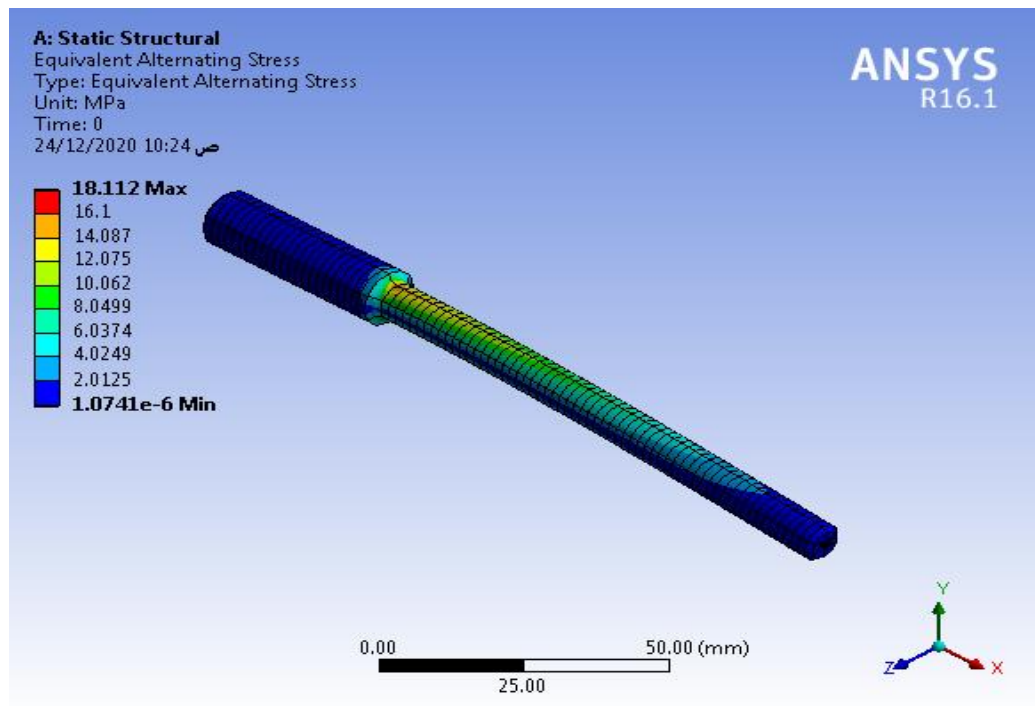
The numerical model used to find equivalent alternating stress is the stress used to query the fatigue S-N curve after accounting for fatigue loading type R-ratio effects and any other fatigue analysis factors.

The experimental side's moments were applied in a numerical model by determining it using equation (4.1).

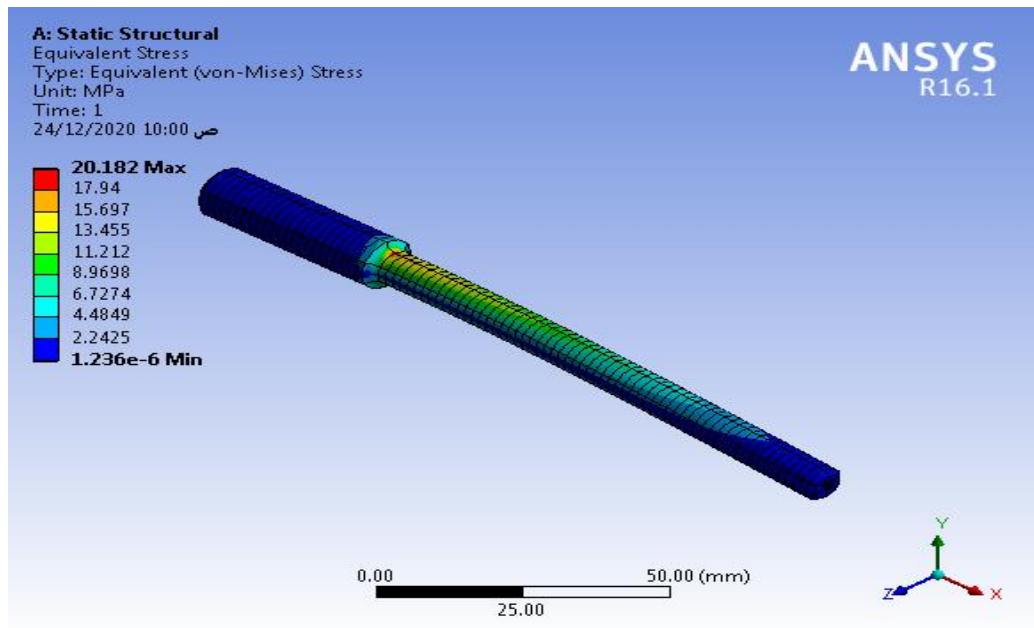
Figures 5.12 shows contour plot of equivalent Von-Mises stress for (0,10,15,20%) wt. R=-1 Von Mises stress is considered for the safe design and gives information if the design fails if the maximum value of Von Mises stress induced in the material is more than the material's strength. It works well for most cases.

Figures 5.13 shows contour plot of safety factor for (0,10,15,20%) wt. at stress ratio R=-1, the maximum safety factor displayed is 15 concerning fatigue failure at given design life. For the fatigue safety factor, values less than 1 indicate failure before the design life was reached.

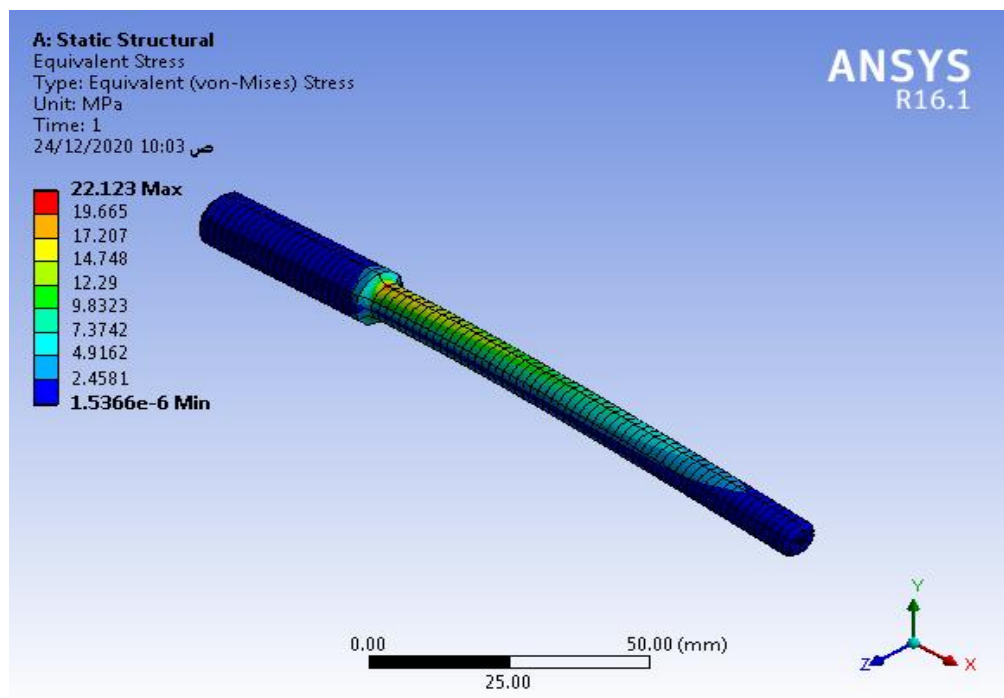
Figure 5.13 shows the contour plot of the life for (0,10,15,20%) wt. obtained for the analysis of fatigue at stress ratio  $R=-1$ . This contour plot shows the given fatigue analysis's available life if the loading of constant amplitude loading represents the number of cycles until the component fails due to fatigue. If the loading of variable amplitude loading, this means the number of loading blocks till failure.



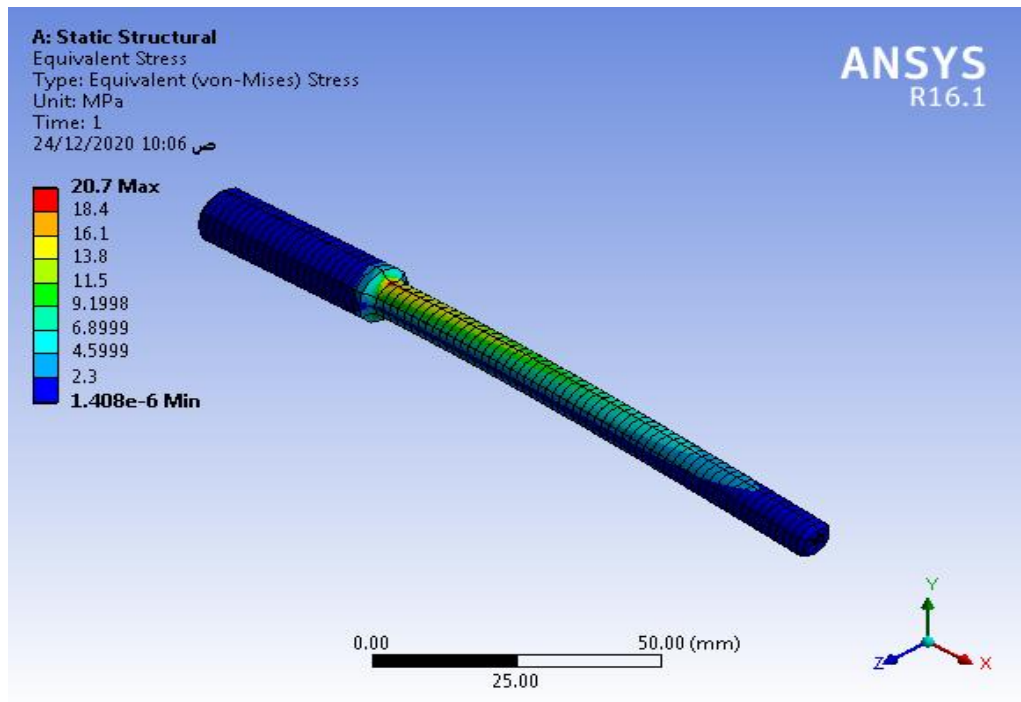
(a) 0% AC



(b) 10% AC

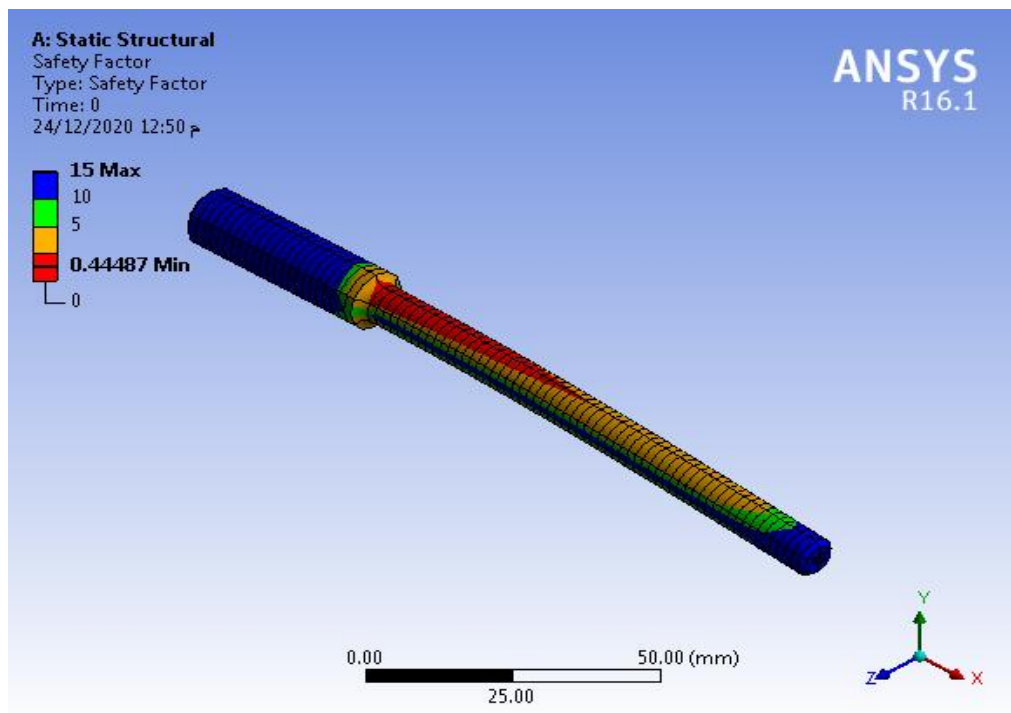


(c) 15% AC

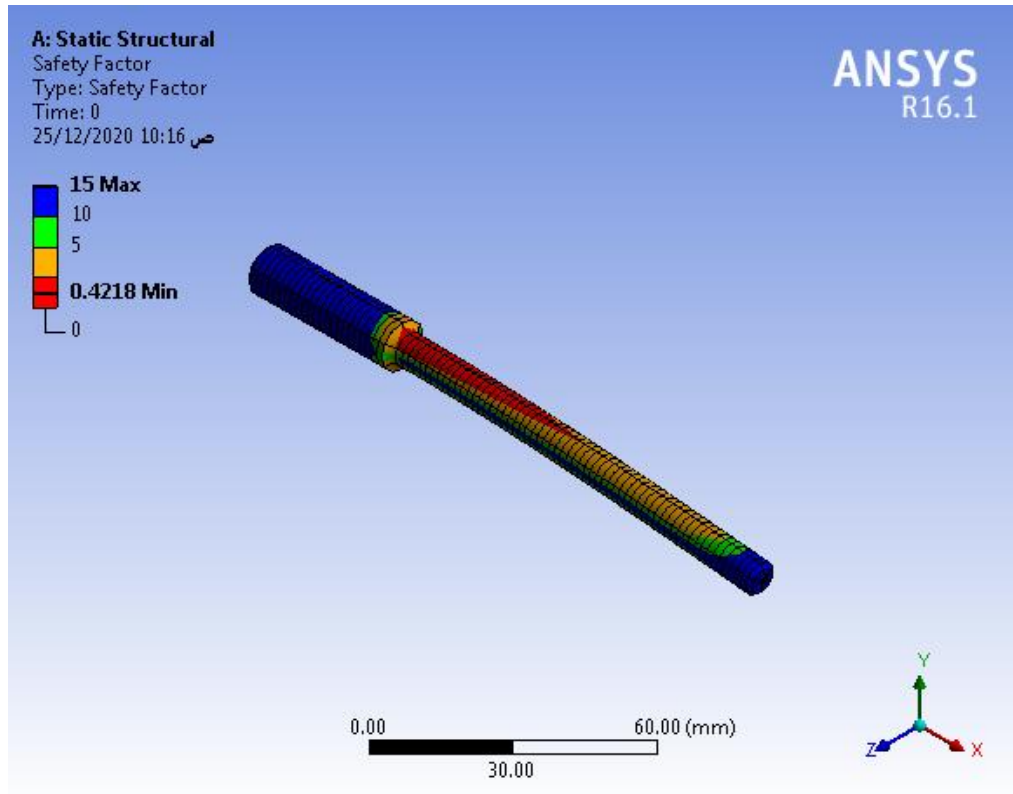


(d) 20% AC

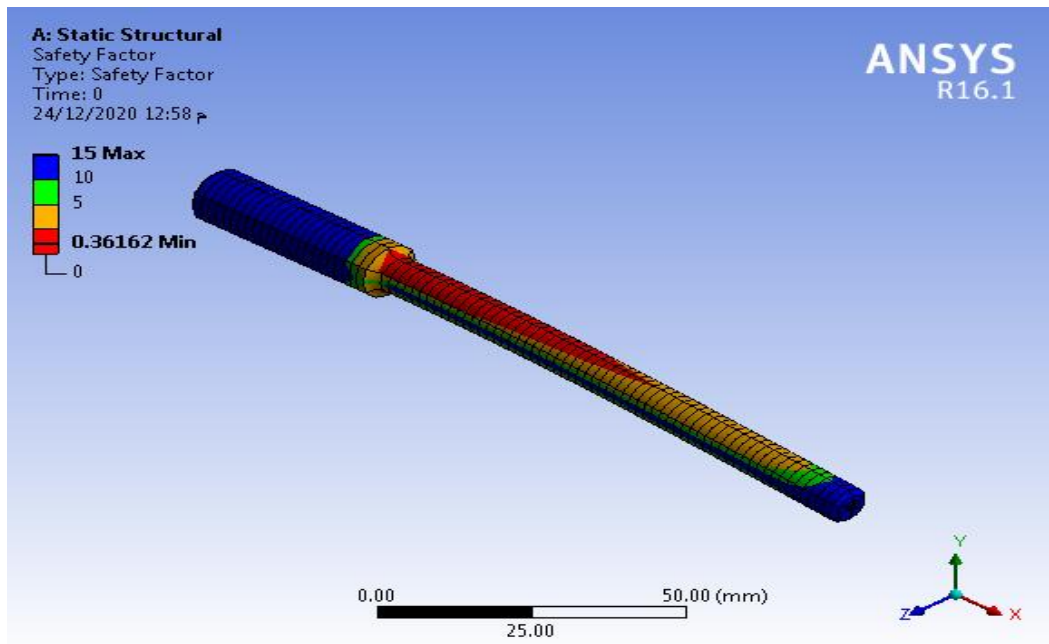
Figure 5.12 Contour plot of equivalent Von-Mises stress at R=-1



(a) 0% AC

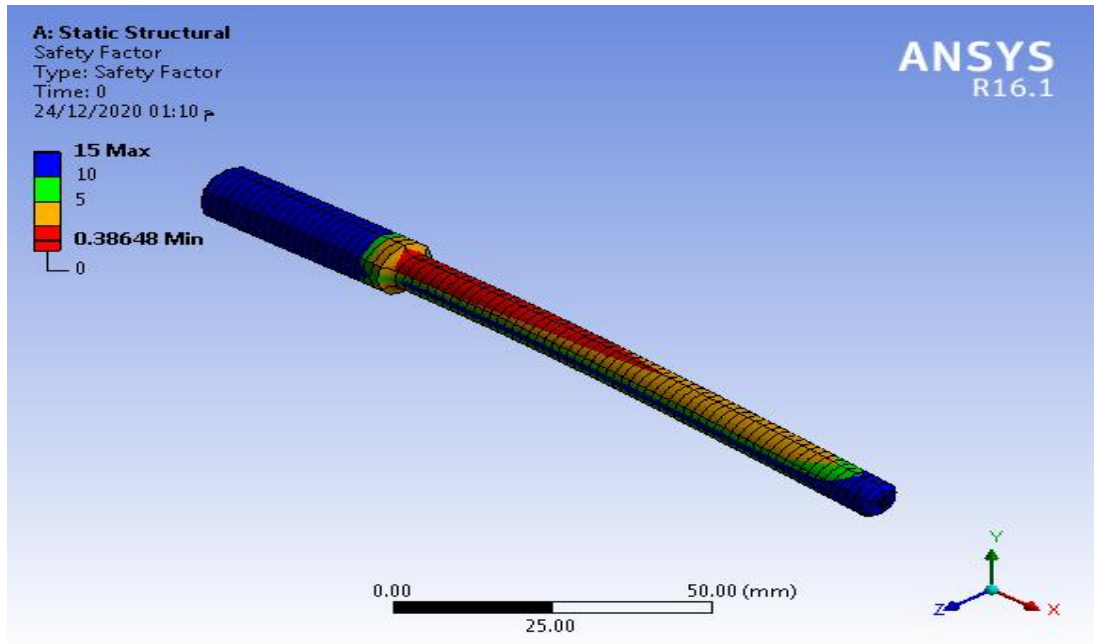


(b) 10% AC



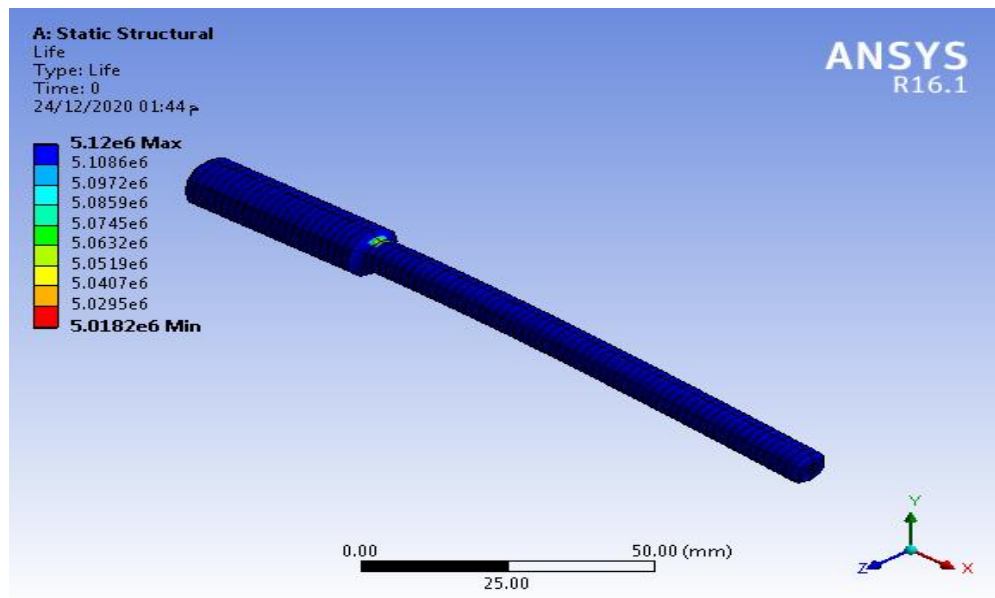
(c) 15% AC



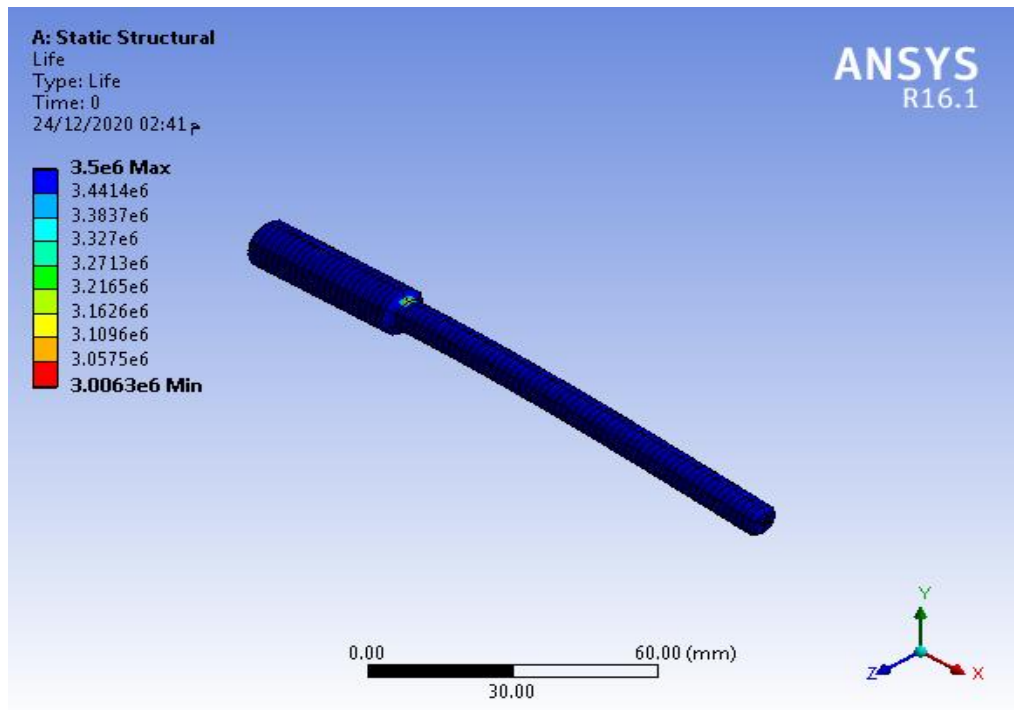


(d) 20% AC

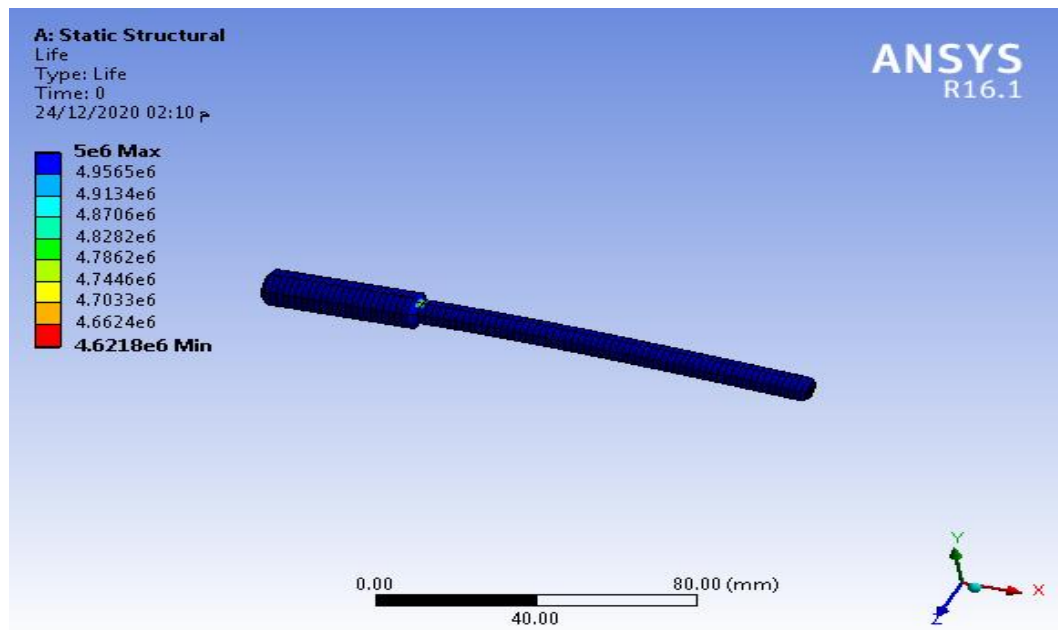
**Figure 5.13** Contour plot of a safety factor, where the maximum safety factor displayed is 15 at stress ratio  $R=-1$ .



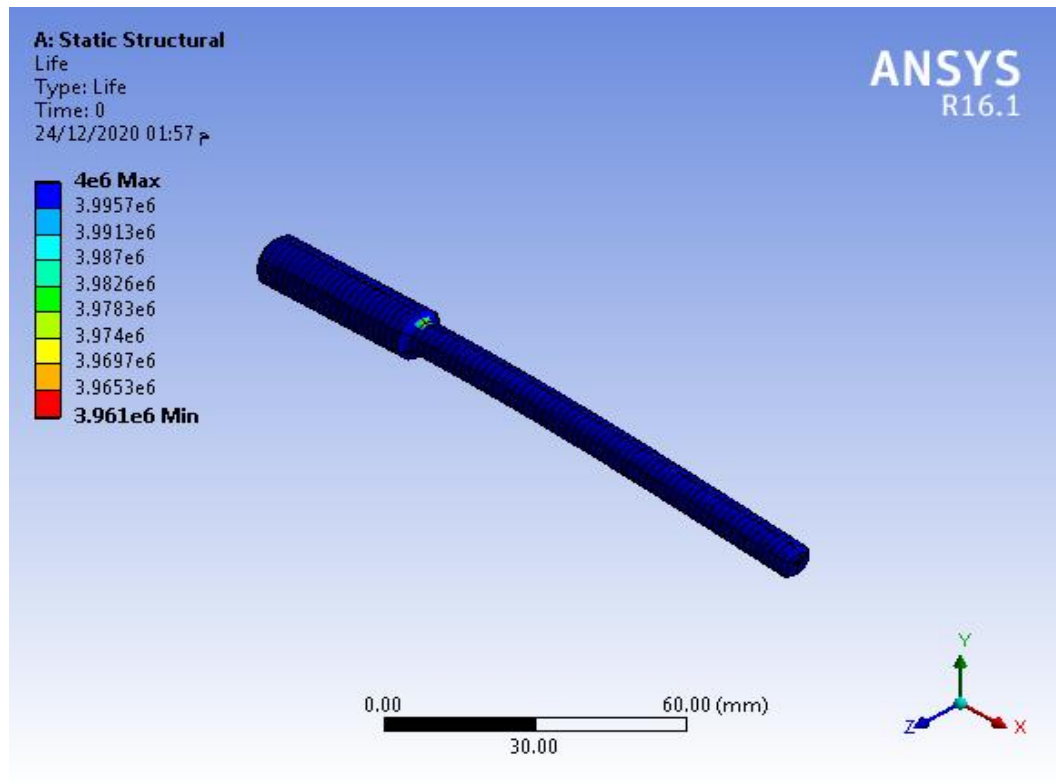
(a) 0% AC



(b) 10% AC



(c) 15% AC



(d) 20% AC

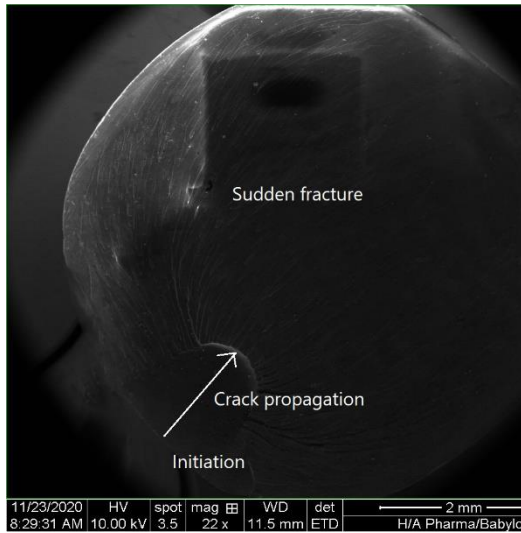
**Figure 5.14** Contour plot of the life obtained for the analysis of fatigue at stress ratio  $R=-1$ .

### 5.7.5 SEM results for fracture surface of fatigue specimens

SEM observed the fracture surfaces of the fractured specimens. It is clear that the fatigue region in the 0% wt. composite, as shown in figure 5.15 (a), has brittle fracture behavior, and the crack initiation region on the surface, crack propagation, sudden fracture region is apparent. In figure 5.15 (b), (c), (d), the fracture has brittle fracture behavior, but fatigue fracture regions not clear due to the presence of activated carbon particles because of its brittleness nature.

By examining fracture surfaces at higher magnifications, the agglomeration is evident in figure 5.16 (c). These flaws were formed typically from incomplete penetration of the matrix material into the particle clusters. The size of dimples

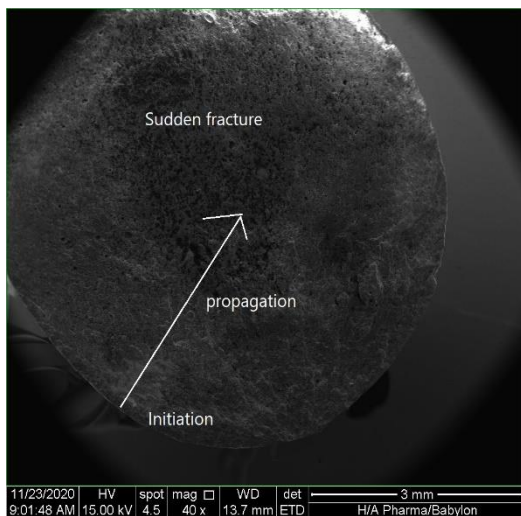
that formed in fractured surfaces decreased by the amount of reinforcement, as shown in figure 5.16 (a), (b), (c).



(a)



(b)

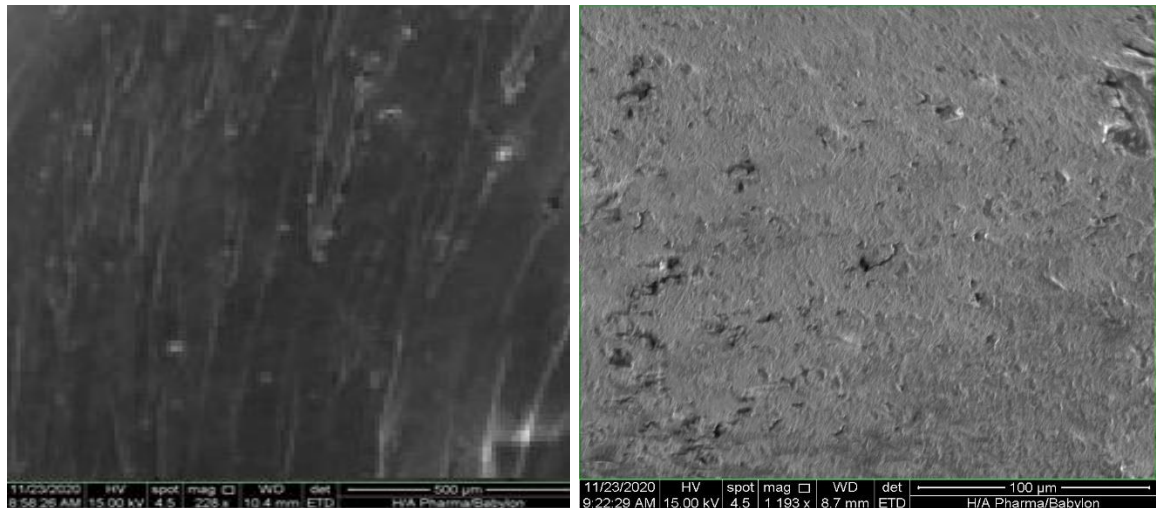


(c)



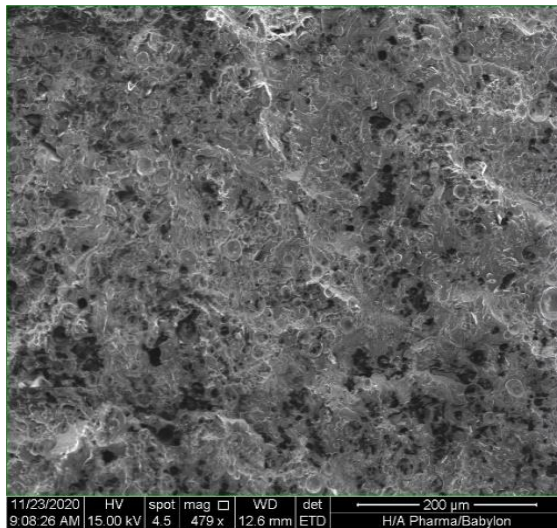
(d)

**Figure 5.15** Micrographs by Scanning electron microscope (SEM) images of fracture surfaces of fatigue specimens for (a) 0 % wt. of activated carbon (b) 10 % wt. of activated carbon (c) 15 % wt. of activated carbon (d) 20 % wt. of activated carbon.

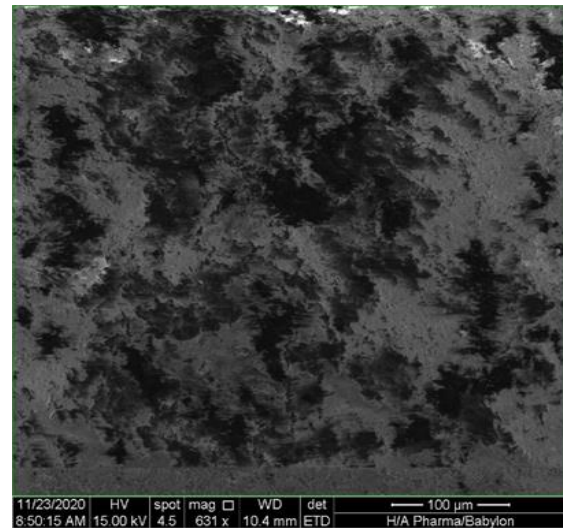


(a)

(b)



(c)



(d)

**Figure 5.16** Micrographs by Scanning electron microscope (SEM) images of fracture surfaces of fatigue specimens for (a) 0% wt of activated carbon (b) 10 % wt. of activated carbon (c) 15 % wt. of activated carbon (d) 20 % wt. of activated carbon.

---

## CHAPTER SIX

### Conclusion and Recommendation

#### 6.1 Introduction

This chapter aims to present the conclusions drawn from the analysis of the experimental and numerical works, focus on the critical discussions, and then make recommendations for further research.

#### 6.2 Conclusions

In this work, the effects of adding activated carbon (AC) powder with (0, 5, 10, 15, 20, 25, 30, 35, 40 %) wt. on epoxy resin were investigated experimentally for tensile tests and (0,10,15,20%) wt. experimentally and numerically for fatigue tests. According to the results obtained from the Laser particle size analyzer, FTIR, DSC, tensile, fatigue and SEM tests, it can be concluded that:

1. There is no new peak or peak shifting after reinforcing the epoxy with activated carbon powder. The bonding type between the matrix and the reinforcement material was a physical bonding, which indicates no new material formed.
2. The glass transition temperature increased with increasing the activated carbon content. Tg's maximum value is 192.83°C which is obtained for composite specimen reinforced with 40% of activated carbon powder.
3. The ultimate tensile strength and elastic modulus of pure epoxy improved with activated carbon powder until it reaches the maximum value at 15 % wt. for ultimate tensile strength and elastic modulus, respectively, as compared with pure epoxy.

4. The strain decreased with the increasing of activated carbon powder because of activated carbon's brittleness nature.
5. The composites failed in a brittle manner, and 15 % wt. of activated carbon powder had the best structure.
6. The increasing in activated carbon weight fraction caused increasing fatigue strength until reaching the maximum value at 15% wt. fraction .
7. The numerical and experimental results showed a good agreement with the maximum difference of about 4.43%.
8. The safety factor value was between 0 and 15 regarding fatigue failure at the given design life. For a fatigue safety factor, values less than 1 indicate failure before the design life was reached, and this not happened.

### **6.3 Recommendation for Future Work**

1. Study the effect of particles type, size, nanoparticles, and shapes that reinforced polymeric materials.
2. Study the effect of varying matrix materials by using thermoplastic polymer.
3. Study the effect of temperature variation on the fatigue properties under variable amplitude loading.
4. Study the effect of adding fibers to fabricate (hybrid composite).
5. Study the effect of stress ratio on fatigue behavior experimentally and numerically.

## References

- [1] JONES, Robert., "Mechanics of composite materials", CRC Press, pp. 8-50, 1998.
- [2] Ru-Min W., Shui-Rong Z., and Ya-Ping Z., "Polymer matrix **composites** and technology", Elsevier, pp. 1-50, 2011.
- [3] Valery V., Vasiliev and Evgeny I, "Mechanics and analysis of composite materials", Elsevier, pp. 1-300, 2001.
- [4] Ajit Kumar S., Subham C., Snehanu S., Ravi R., Subhashis N., and Amit K., "Mechanical and Tribological Analysis of Polymer Matrix Composites". *Int. J. Eng. Adv. Technol*, pp. 193-203, (2017).
- [5] Josmin P., Sant K., Sabu T., Kuruvilla J., Koichi G., and Meyyarappallil S. "Advances in polymer composites: macro-and micro composites—state of the art, new challenges, and opportunities" *Polymer Composites*; Wiley: Weinheim, Germany, *1*, pp. 3-16, 2012.
- [6] Eric Paul L., " Production, characterization, and applications of activated carbon, "Doctoral dissertation, University of Missouri—Columbia, pp. 1-66, 2010.
- [7] Tadda, M. A., Ahsan, A., Shitu, A., ElSergany, M., Arunkumar, T., Jose B. and Daud, N. N. "A review on activated carbon: process, application and prospects. *Journal of Advanced Civil Engineering Practice and Research*", 2(1), pp.7-13, (2016).
- [8] Saeidi, N., and Lotfollahi, M. "Effects of powder activated carbon particle size on adsorption capacity, and mechanical properties of the semi activated carbon fiber. *Fibers and Polymers*", 16(3), pp. 543-549. (, 2015).
- [9] Devi, A. H., & Kumar, G. V., "Fatigue Performance and damage mechanisms of Reinforced Polymer Composites-A Review", *International Research Journal of Engineering and Technology (IRJET)*, pp. 1-7, 2016.



## References

---

- [10] Ajaj E. A., Jubier N. J., and Majeed K. J., "Fatigue behavior of epoxy/SiO<sub>2</sub> nanocomposites reinforced with E-glass fiber. *International Journal of Application or Innovation in Engineering & Management*", 2(9), pp. 61-70, 2013.
- [11] Agunsoye J. O., Isaac T. S. and Samuel S. O., "Study of mechanical behavior of coconut shell reinforced polymer matrix composite", *Journal of minerals and materials characterization and Engineering*, 11(8), pp. 774-779, 2012.
- [12] Salleh Z., Islam M. M., Yusop M. Y., and Idrus M., "Mechanical properties of activated carbon (AC) coconut shell reinforced polypropylene composites encapsulated with epoxy resin", *APCBEE procedia*, 9, pp. 92-96, 2014.
- [13] Atuanya C. U., Nwaigbob S. C., and Igbokwec P. K., "Effects of breadfruit seed hull ash particles on microstructures and properties of recycled low-density polyethylene/breadfruit seed hull ash composites", *Scientia Iranica*, 21(3), pp.792-802, 2014.
- [14] Islam M. M., Kabir H., Gafur M. A., Bhuiyan M. M. R., Kabir M. A., Qadir M. R., and Ahmed F., "Study on physio-mechanical properties of rice husk ash polyester resin composite", *International Letters of Chemistry, Physics and Astronomy*, 53, pp. 95-105, 2015.
- [15] Salman J. M., "Studying Some Properties of Unsaturated Polyester Composite Reinforced by Carbon Black Particulate", *Journal of the University of Babylon*, 23(2), 271-275, 2015.
- [16] Islam I., Sultana S., Kumer Ray S., Parvin Nur H., and Hossain M., "Electrical and tensile properties of carbon black reinforced polyvinyl chloride conductive composites", *C—Journal of Carbon Research*, 4(1), pp. 15, 2018.

## References

---

- [17] Costa Dias T. da, Panzera T. H., Freire R. T. S., C. T. Garcia, and J. C. dos Santos, "EPOXY POLYMERS REINFORCED WITH CARBON POWDER WASTES", Brazilian Conference on Composite Materials, 2018.
- [18] Seth S. A., Aji A. T. I. S., and Nigeria B., "Investigation of the Impact, Hardness, Density and Water absorption of Polypropylene Filled Doum Palm Shell Particles Composite", Journal of Information Engineering and Applications, 2019.
- [19] Khalil H. A., Noriman N. Z., Ahmad M. N., Ratnam M. M., and Fuaad N. N., "Polyester composites filled carbon black and activated carbon from bamboo (*Gigantochloa scortechinii*): Physical and mechanical properties", Journal of
- [20] Laouchedi D., Bezzazi B., and Aribi, C. "Elaboration and characterization of composite material based on epoxy resin and clay fillers", Journal of applied research and technology, 15(2), pp. 190-204, 2017.
- [21] Abdullah O. S., "Experimental Study to the Effect of Natural Particles Added to Unsaturated Polyester Resin of a Polymer Matrix Composite", Al-Khwarizmi Engineering Journal, 13(1), 42-49, 2017.
- [22] Hardinnawirda K., and SitiRabiatull Aisha I., "Effect of rice husks as filler in polymer matrix composites", Journal of Mechanical Engineering and Sciences, 2, pp. 181-6, 2012.
- [23] Ojha S., Raghavendra G., and Acharya S. K., Fabrication and study of mechanical properties of orange peel reinforced polymer composite ", Caspian Journal of Applied Sciences Research, 13, 0-6, 2012.
- [24] Shakuntala O., Raghavendra G., and Samir Kumar A., "Effect of filler loading on mechanical and tribological properties of wood apple shell reinforced epoxy composite", Advances in Materials Science and Engineering, 2014.

- [25] Abass, R. U., "Mechanical Behavior of Natural Material (Orange Peel) Reinforced Polymer Composite International", Journal of Engineering Science & Research Technology, 2015.
- [26] Salasinska K., Barczewski M., Górny R., and Kloziński A., "Evaluation of highly filled epoxy composites modified with walnut shell waste filler", Polymer Bulletin, 75(6), pp. 2511-2528, 2018.
- [27] Mohammed R. A., and Al-Ghabban A., "Mechanical Properties of Poly Methyl Methacrylate Filled with Orange Peels", Zanco Journal of Pure and Applied Sciences, 31(s3), pp. 106-113, 2019.
- [28] Haque M. M. U., Goda K., S. Ogoe, and Sunaga Y., "Fatigue analysis and fatigue reliability of polypropylene/wood flour composites", Advanced Industrial and Engineering Polymer Research, 2(3), pp.136-142, 2019.
- [29] AL-Ajaj E. A., and Hassan M. H. B., "Fatigue Behavior of Chopped Carbon Fiber Reinforced Epoxy Composites", Iraqi Journal of Physics, 8(11), pp.110-117, 2010.
- [30] Shokrieh M. M., Esmkhani M., and Haghightakhah A. R., "Mechanical properties of graphene/epoxy nanocomposites under static and flexural fatigue loadings", Mechanics of Advanced Composite Structures, 1(1), pp. 1-7, 2014.
- [31] William Casllister D., "Materials science and engineering an introduction", 5 th edition, Wiley and Sons Inc, 2000.
- [32] Ajaj E. A., Jubier N. J., and Majeed K. J., "Fatigue behavior of epoxy/SiO<sub>2</sub> nanocomposites reinforced with E-glass fiber", International Journal of Application or Innovation in Engineering & Management, 2(9), pp. 61-70, 2013.
- [33] Ibrahim M. E. I. M. E., "Modelling of the Stresses and Deflection Distribution in Airport Rigid Pavement Using Finite Element Analysis" Doctoral dissertation, Sudan University of Science Technology, 2019.

## References

---

- [34] Kailas S. V., "Material Science", Indian Institute of Science,
- [35] Kumbhar S. V., and Tayade R. M., "A case study on the effect of mean stress on fatigue life", *International Journal of Engineering Development and Research*, 2(1), 304-308, 2014.
- [36] Sharma, A., Oh, M. C., and Ahn, B." Recent Advances in Very High Cycle Fatigue Behavior of Metals and Alloys"10(9), 1200, (2020).
- [37] Shekunov B. Y., Chattopadhyay P., Tong H. H., and Chow A. H., "Particle size analysis in pharmaceuticals: principles, methods and applications", *Pharmaceutical Research*, 24(2), 203-227, 2007.
- [38] ASTM, A 2014 D638-14 Standard Test Method for Tensile Properties of Plas-1010 Tics (ASTM International).
- [39] G.U.N.T, "WP 140 Fatigue Testing Apparatus", Publication No.:912.00000A 140 12, [www.gunt,http://www.gunt.de](http://www.gunt.de), 2009.
- [40] Ali H.," Effect of variation in temperature on the fatigue properties of steel with different carbon contains , MSc thesis submitted to the university of Babylon ,collage of engineering, pp.41,2018.
- [41] Yin Q., Yang W., Sun C., and M. Di, "Preparation and properties of lignin-epoxy resin composite", *BioResources*, 7(4), 5737-5748, 2012.
- [42] Doblies A., Boll B., and Fiedler B., "Prediction of thermal exposure and mechanical behavior of epoxy resin using artificial neural networks and Fourier transform infrared spectroscopy", *Polymers*, 11(2), pp. 363, 2019.
- [43] Chen J., Kinloch A. J., Sprenger S., and Taylor A. C., "The mechanical properties and toughening mechanisms of an epoxy polymer modified with polysiloxane-based core-shell particles", *polymer*, 54(16), pp. 4276-4289, 2013.
- [44] Qi B., S. R. Lu, Xiao X. E., Pan L. L., Tan F. Z., and Yu J. H., "Enhanced thermal and mechanical properties of epoxy composites by mixing

## References

---

- thermotropic liquid crystalline epoxy grafted graphene oxide", *Express Polymer Letters*, 8(7). (2014).
- [45] Roy P. K., and Ramanan A., "Toughening of epoxy resin using Zn<sub>4</sub>O (1,4-benzene dicarboxylate) <sup>3</sup> metal-organic frameworks", *RSC Advances*, 4(94), 52338-52345, 2014.
- [46] Hunain M. B., "Experimental and theoretical study of composite material under static and dynamic loading with different temperature condition ", doctorate thesis submitted to University of Technology, 2014.

## Appendix A-1

### Differential scanning calorimetry DSC Results

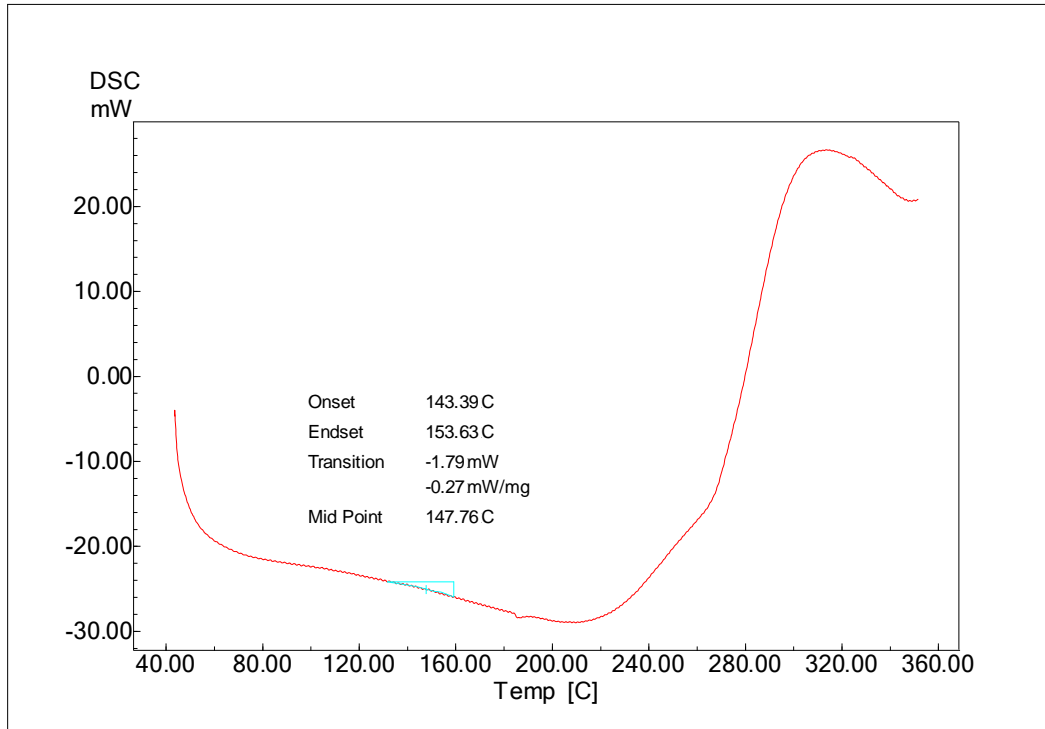
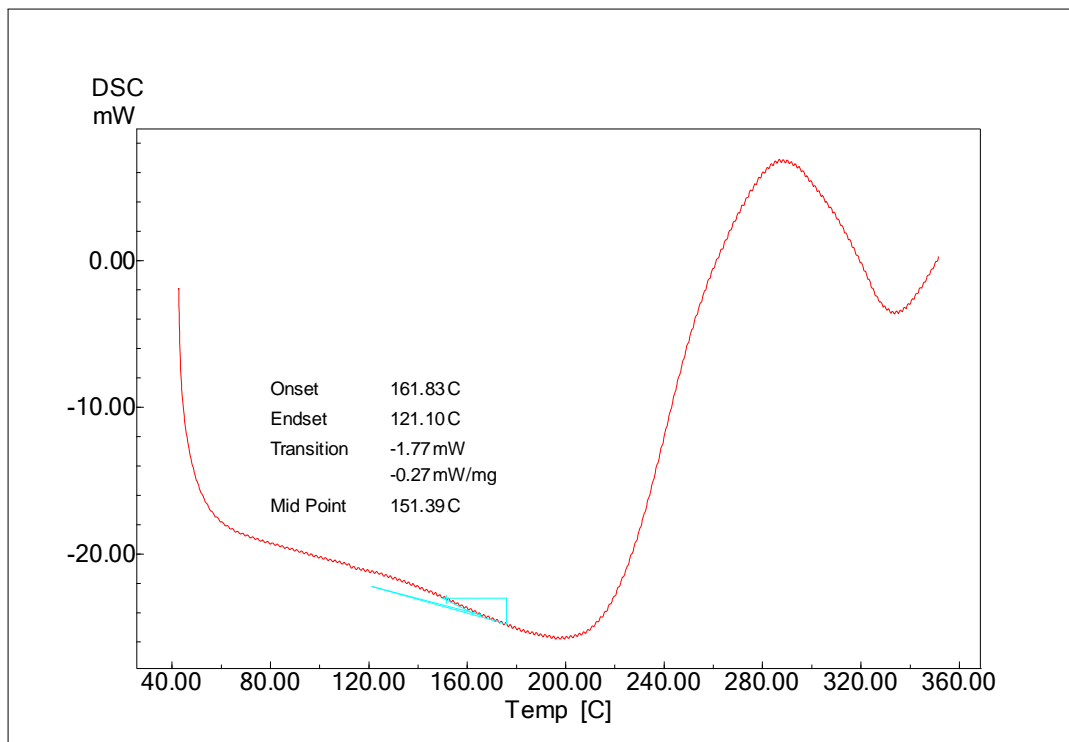
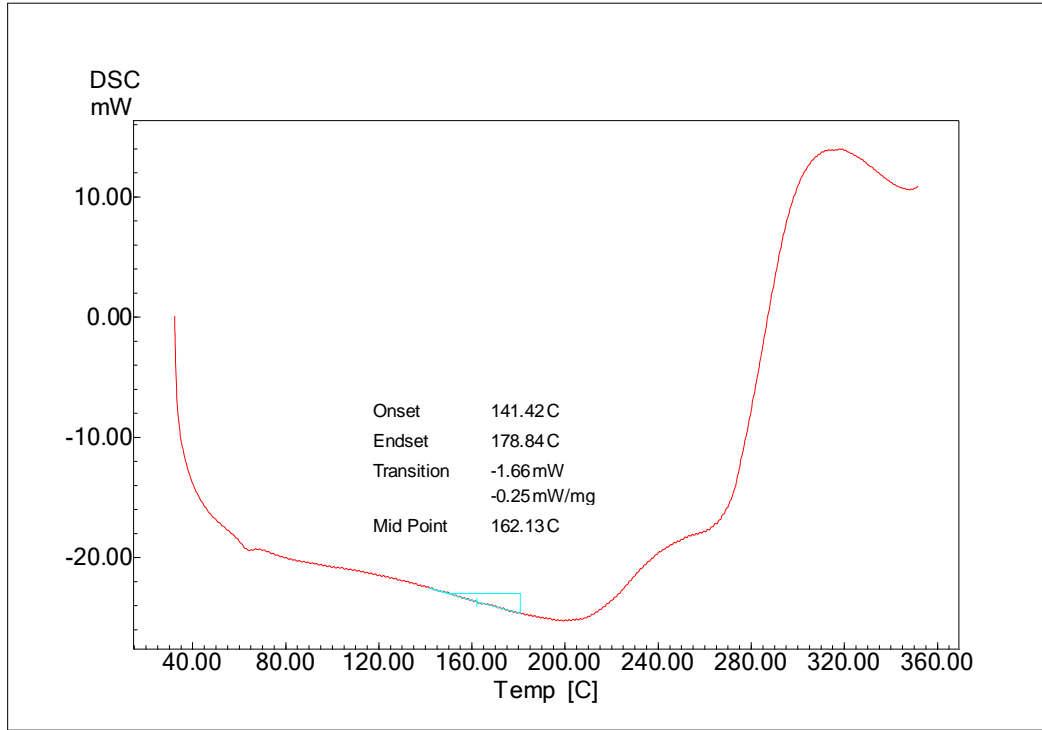


Figure A-1 DSC results for 0% wt.



**Figure A-2** DSC results for 5% WT.



**Figure A-3** DSC results for 10% wt.

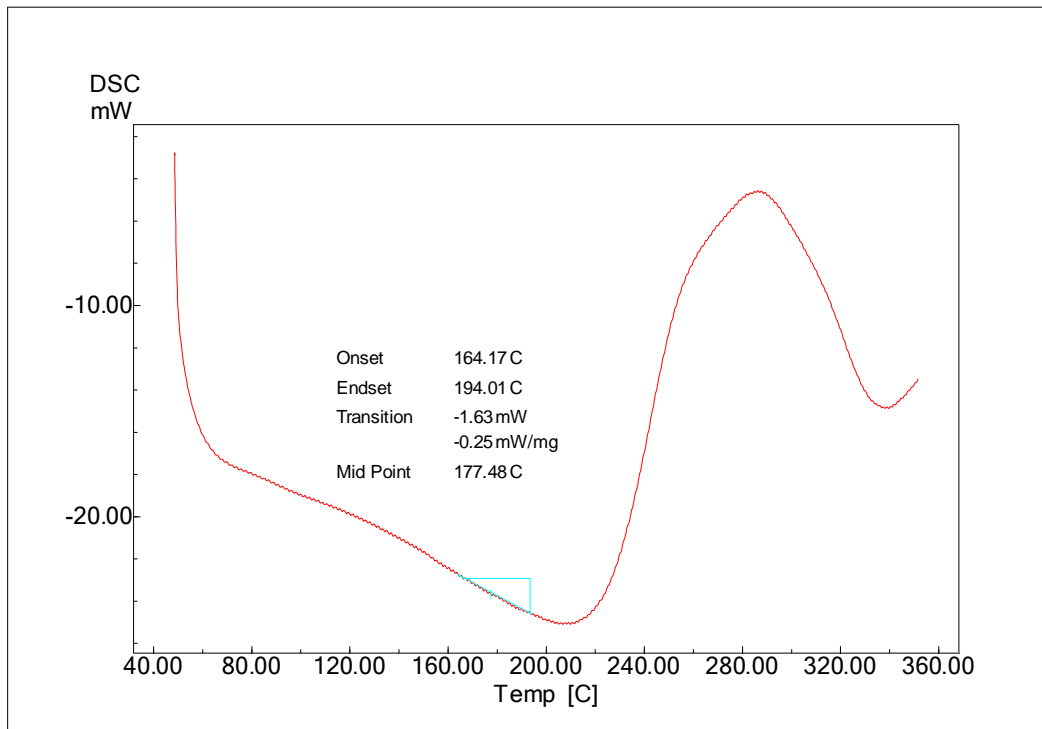


**Figure A-4** DSC results for 15% wt.

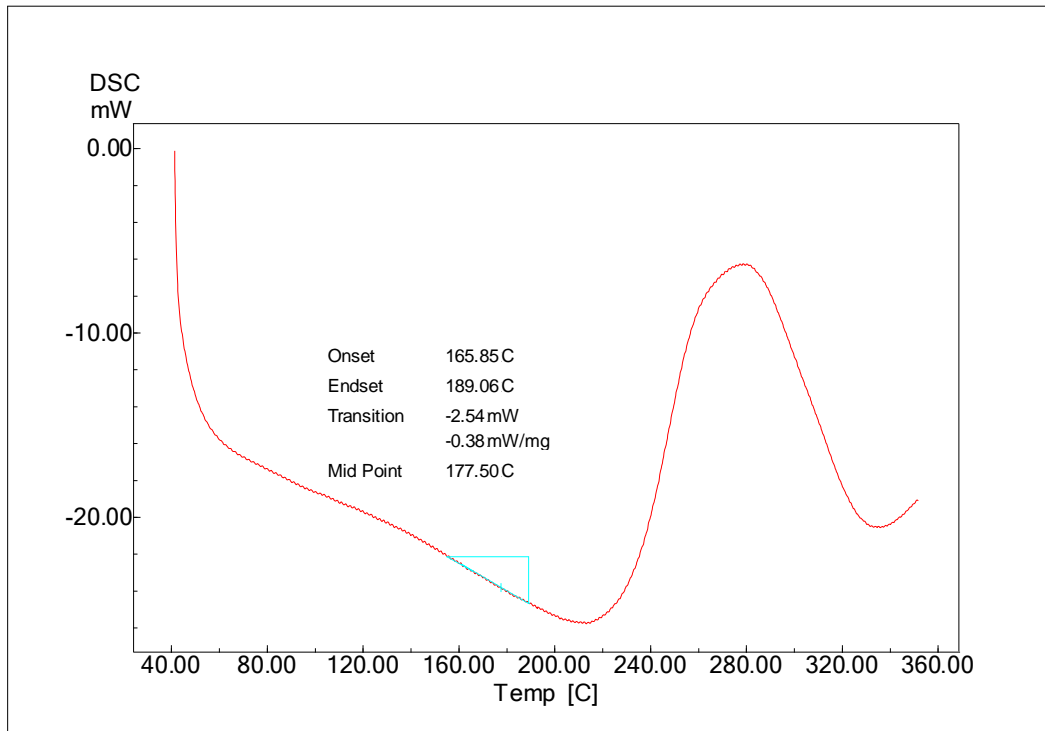


Figure A-5 DSC results for 20% wt.

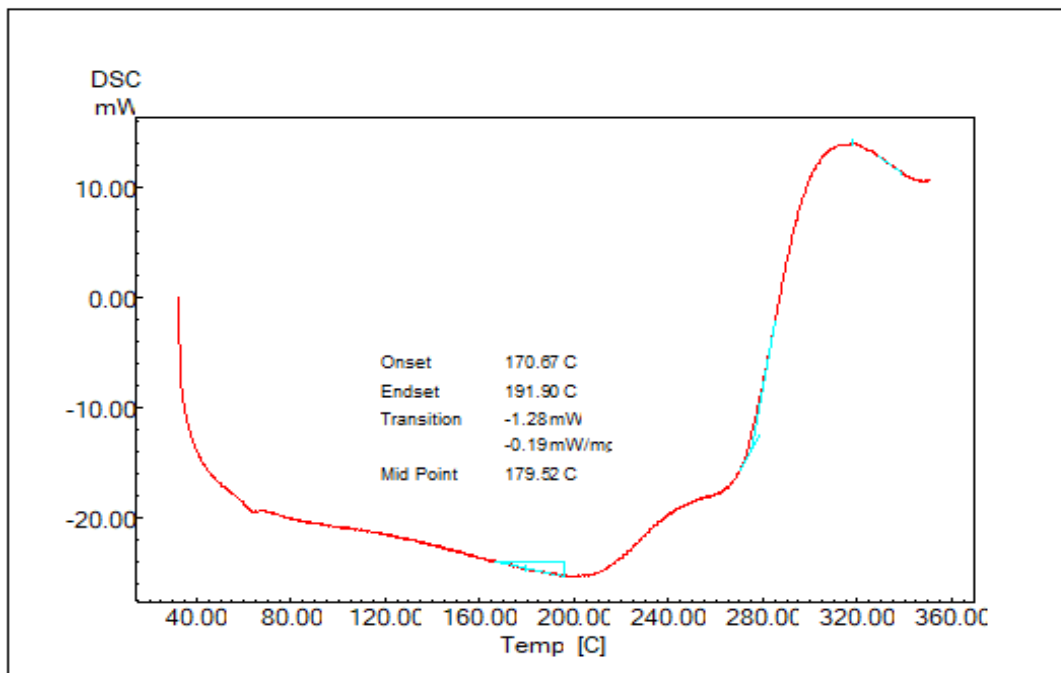
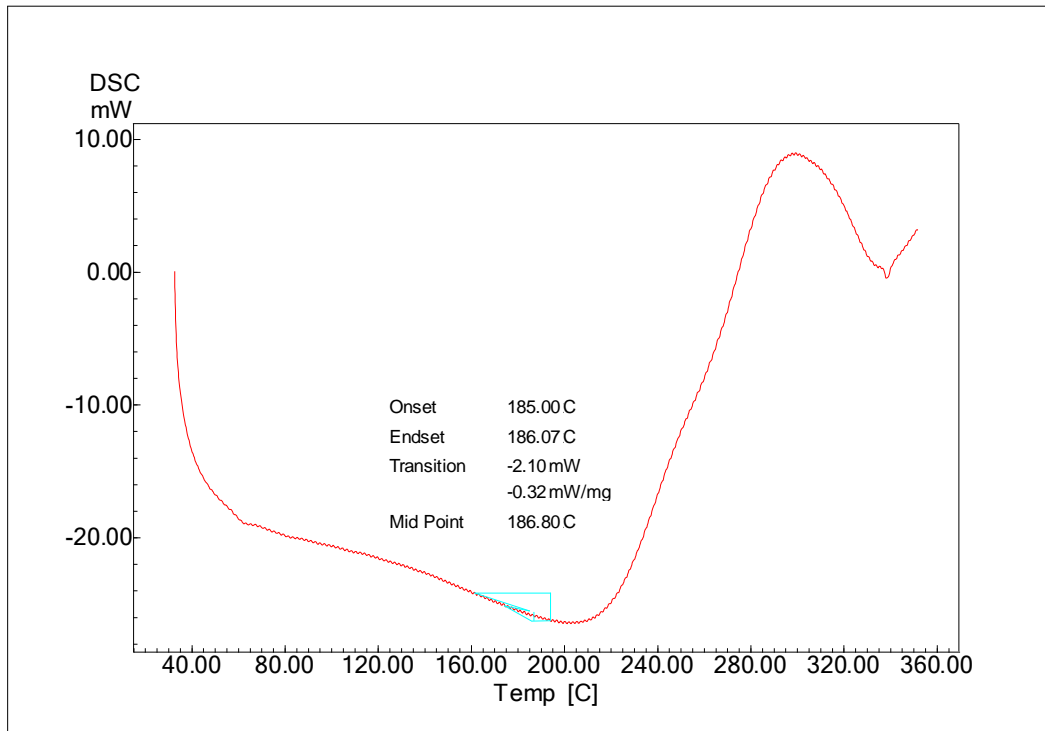
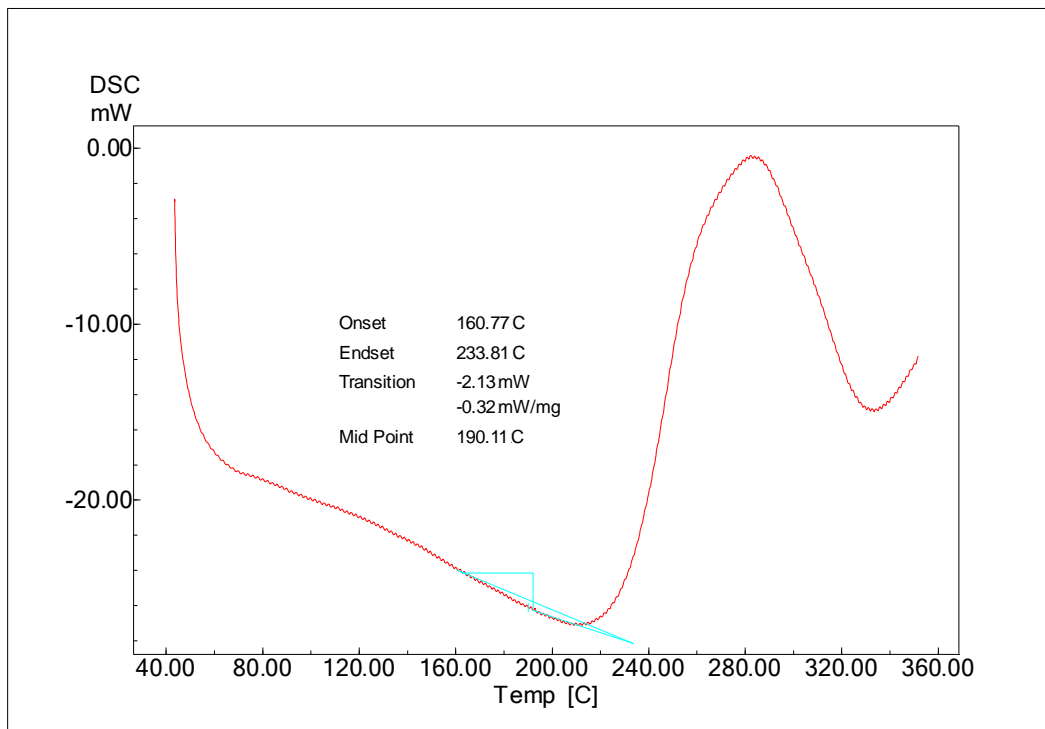


Figure A-6 DSC results for 25% wt.





**Figure A-7** DSC results for 30% wt.



**Figure A-8** DSC results for 35% wt.

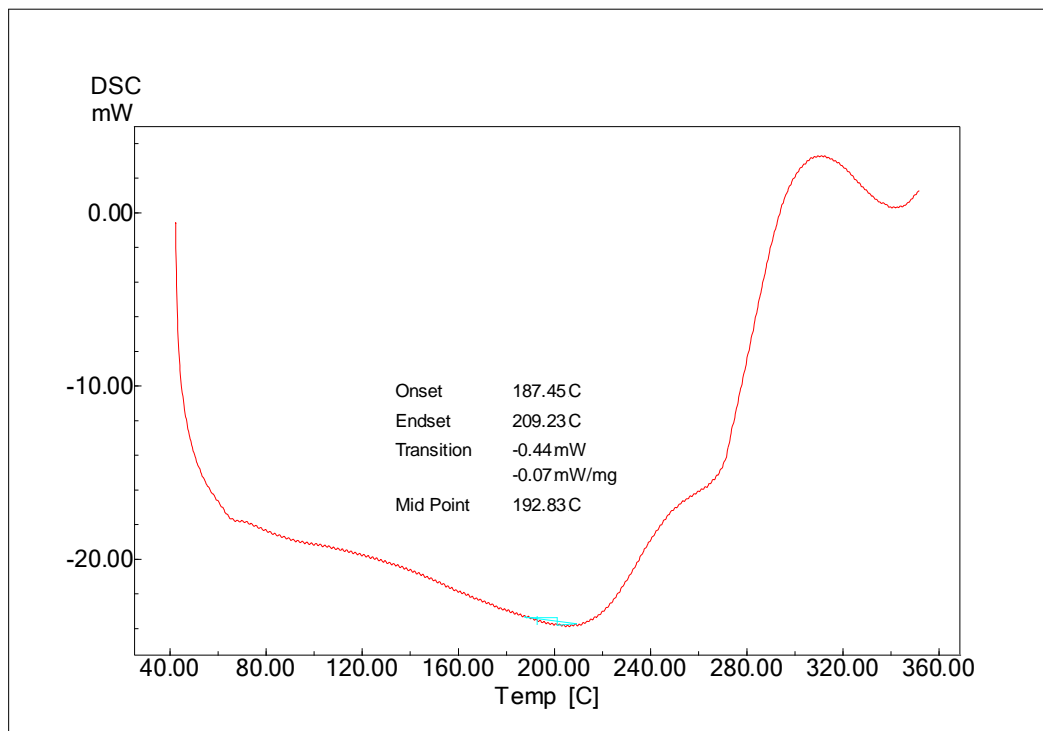


**Figure A-9** DSC results for 40% wt.

## الخلاصة

استخدام المدعمات مع المواد البوليمرية كالكربون الفعال (AC) كبديل للمواد الصناعية هو موضوع مهم هذه الأيام هذه المدعمات ذات القاعدة النباتية هي متحللة، صديقة للبيئة، وفيرة ورخيصة بينما المواد الصناعية مكلفة ولها تأثير سلبي على البيئة.

في هذا العمل تم دراسة تأثير إضافة باودر الكربون الفعال الى راتنج الايبوكسي وبحث تجريبيا ونظريا. المواد المركبة الحبيبية صنعت بتقنية التفريغ لعدة نسب وزنية من باودر الكربون الفعال (0،5،10،15،20،25،30،35،40%) لإيجاد أفضل نسبة إضافة التي تعطي أفضل الخواص الميكانيكية وخواص الكلال.

حجم الحبيبات تم قياسه خلال هذا العمل بجهاز محلل الحجم الليزري وهو 14,74 مايكرومتر. التماسك بين مادة الايبوكسي وباودر الكربون الفعال فحص باستخدام مطياف فورييه للتحليل الطيفي بالأشعة تحت الحمراء (FTIR) ، علاوة على ذلك تم قياس درجة حرارة التزجج للايبوكسي النقي والمواد المركبة بجهاز فرق المسح الكالوري (DSC).

سلوك مقاومة الشد والكلال تمت دراسته تجريبيا ونظريا، سلوك الكلال تم وصفه بمنحنى (S-N) باستخدام معادلة (Basquin's Equation). العمل النظري تم باستخدام برنامج الانسسز.

البنية الجزيئية للمواد المركبة والترابط بين المادة الأساس والحبيبات تم بواسطة فحص الكسر لعينات الشد والكلال باستخدام المجهر الالكتروني (SEM) لاطهار الكسر الناتج في هذه المركبات.

نتائج ال (FTIR) أظهرت انه لا يوجد قمم جديدة بعد تدعيم الايبوكسي بباودر ال (AC) والذي يثبت الترابط القوي بين الايبوكسي وباودر ال (AC).

نتائج ال (DSC) أظهرت زيادة بدرجة حرارة التزج بإضافة الباودر الى الايبوكسي

نتائج ال (FTIR) دعمت بواسطة نتائج المجهر الالكتروني الذي اظهر ترابط جيد وقوي التداخل قوية بين المادة الأساس والباودر.

مقاومة الشد ازدادت مع زيادة باودر الكاربون الفعال الى نسبة ال 15% لاعظم قيمة 26,34 ميكا باسكال ازدادت بمقدار 18,87% وبعدها تناقص الى 18,15 ميكا باسكال عند نسبة 40%.

مقاومة الكلال العظمى ازدادت أيضا بزيادة حبيبات ال (AC) ليصل الى أعظم قيمة عند ال 15%.

تقنية ال (3D Finite Element) استخدمت لنمذجة اختبار الكلال نظريا باستخدام برنامج (ANSYS work bench) لمقارنة منحنيات ال (S-N) والتي امتلكت نفس السلوك وكانت اعظم نسبة مئوية للفرق بينهما لا تزيد عن (4,43%) كذلك استخدم هذا البرنامج لإيجاد عمر الكلال بمعامل الأمان، و اجهاد (Von-Mises).

أخيرا استخدم المجهر الالكتروني (SEM) لفحص البنية المجهرية ولإظهار طبيعة الكسر.



جمهورية العراق  
وزارة التعليم العالي والبحث العلمي  
جامعة كربلاء  
كلية الهندسة / قسم الميكانيك

# سلوك الكتل للمواد المركبة البوليمرية المدعمة بحبيبات الكربون الفعال.

رسالة

مقدمة الى جامعة كربلاء/كلية الهندسة/ قسم الهندسة الميكانيكية  
كجزء من متطلبات نيل درجة الماجستير في الهندسة الميكانيكية (ميكانيك  
تطبيقي)

من قبل:

قبس رزاق عبد علي

باشراف

الأستاذ المساعد الدكتور

مصطفى باقر هنين

الأستاذ المساعد الدكتور

صلاح نوري النعماني

